Modelling the thermal characteristics of a greenhouse coupled with a solar thermal heating system

James Philbrick

Submitted in partial fulfilment of the requirements
for the degree of Mechanical Engineering BA (Hons)

School of Engineering, University of Lincoln

Dr Amir Badiee

May 2022

UNIVERSITY OF
LINCOLN

Contents

Nomenclature

α	Absorption of the cover; empirical heat transfer coefficient
β_i	Slope of surface i relative to horizontal
δ	Declination
η	Efficiency factor; scalar value
γ_s	Elevation of the sun
Gr	Grashof number
μ	Absolute (dynamic) viscosity
ν	Kinematic viscosity
Nu	Nusselt number
ω	Solar hour
ϕ	Latitude on earth
Pr	Prandtl number
Ra	Rayleigh number
ρ	Density
σ	Stefan–Boltzmann constant
τ	Transmittance of the cover
θ_i	The angle of incidence for beam radiation with respect to surface i
θ_z	Zenith angle
E	Emissivity coefficient
F_{a_b}	View factor between surface a and b
f_{diff}/f_{dif}	Fraction of diffuse radiation
G_{on}	Extraterrestrial irradiance
h	convective heat transfer coefficient
I	Solar irradiance
k	Thermal conductivity
k_t	Clearness index
N_a	Number of air changes per hour
R_b	Proportion of beam radiation incident on a surfaces with respect to the horizontal
$R_{d,r}$	View factor of a surface relative to the sky and ground respectively

rh Relative humidity

$S(t)$ Solar radiation intensity on an inclined surface

T Temperature

V Volume or volumetric flow rate in the case of V_{ven}

v Wind speed

Structure

c_{p_a} Specific heat capacity ofelement a

Q_{a_b} Heat flow from element a to element b

Subscripts

a Internal air

b Beam radiation component I_b

c cover (glass)

d Diffuse radiation component I_d; dew point in the case of T_d

f Floor of the greenhouse

h Solar thermal heater

o External air T_o; External solar radiation incident on a horizontal plane I_o

rd Radiation transfer

s soil

sk sky

1 List of Figures

2 List of Tables

3 List of Code Listings

4 Preamble

4.1 Acknowledgements

Firstly, I would like to thank my project supervisor, Dr Amir Badiee for his invaluable feedback and guidance throughout this project. I would also like to thank Chris Bingham, Tim Smith, Andrew Moore, and the many friendly and helpful staff members at the Riseholme campus. Furthermore, I am indebted to my fellow student colleagues, Jess Fletcher and Weronika Palka who worked alongside myself as part of the overarching ICaRE4Farms project. I am additionally grateful to John Bowden and my friends and family for their emotional support and reassurances. Last but definitely not least, a gigantic thank you to Abbie Laycock for providing an endless well of support and encouragement and for helping me through the ups and downs as this project progressed.

4.2 Statement of Originality

This dissertation contains no material which has been accepted for a degree or diploma by the University or any other institution, except by way of background information and duly acknowledged in the dissertation, and to the best of my knowledge and belief no material previously published or written by another person except where due acknowledgement is made in the text of the dissertation, nor does the dissertation contain any material that infringes copyright. All images, figures, and diagrams are, unless watermarked or otherwise directly stated, original works.

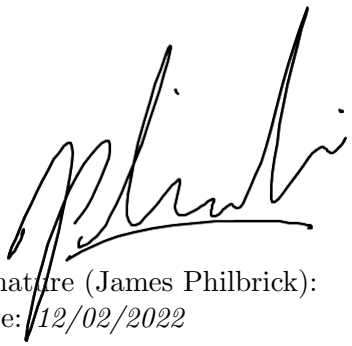

Signature (James Philbrick):
Date: *12/02/2022*

5 Abstract

A mathematical model for predicting the internal temperature, cover (glass) temperature, and floor temperature of a greenhouse is presented. It uses a set of coupled ordinary differential energy balance equations which are solved in MATLAB using a numerical Runge-Kutta technique. The model input takes the form of a series of environmental measurements such as the external air temperature, soil temperature, wind speed, and others; this data was sourced in situ from the greenhouse being modelled as well as from a nearby weather station.

The model was validated with experimental data and the results were deemed inconclusive due to issues regarding data quality and the practical implementation of the models solving environment. Future improvements and areas of investigation are also discussed.

The model prediction reports a maximum error of 20°C and a minimum of 0°C, with an RMSE value of 6.49°C and an MAE value of 4.17°C.

6 Introduction

The ultimate aim of this project was to test the efficiency of new solar thermal collector technology, used for water heating applications, when used to thermally regulate a greenhouse. This new technology is stated to be three times more efficient than traditional STE systems[1,2] [2]; the aim is to investigate if this solar energy captured can be used to heat water by the required amount to be able to sufficiently heat up a greenhouse. The University of Lincoln Riseholme Campus was intended for use as a pilot test site to assess the performance of this technology. Unfortunately, the solar thermal collector was unable to be installed. Initially, logistic issues due to the COVID-19 pandemic resulted in delays in shipping the technology to the site and a further progress impediment was the heritage status held by St Mary's church at Riseholme which introduced difficulties in approving planning permission from Lincoln City Council to construct the system installation[3]. The results and the majority of the methodology in this report therefore do not include the influence of this new solar thermal technology on the thermal dynamics of the greenhouse; rather, only the passive influences such as environmental factors and greenhouse properties are considered and can be modelled and subsequently validated. The greenhouse considered in this report shown in figure 1, with its dimensions given in figure 2.

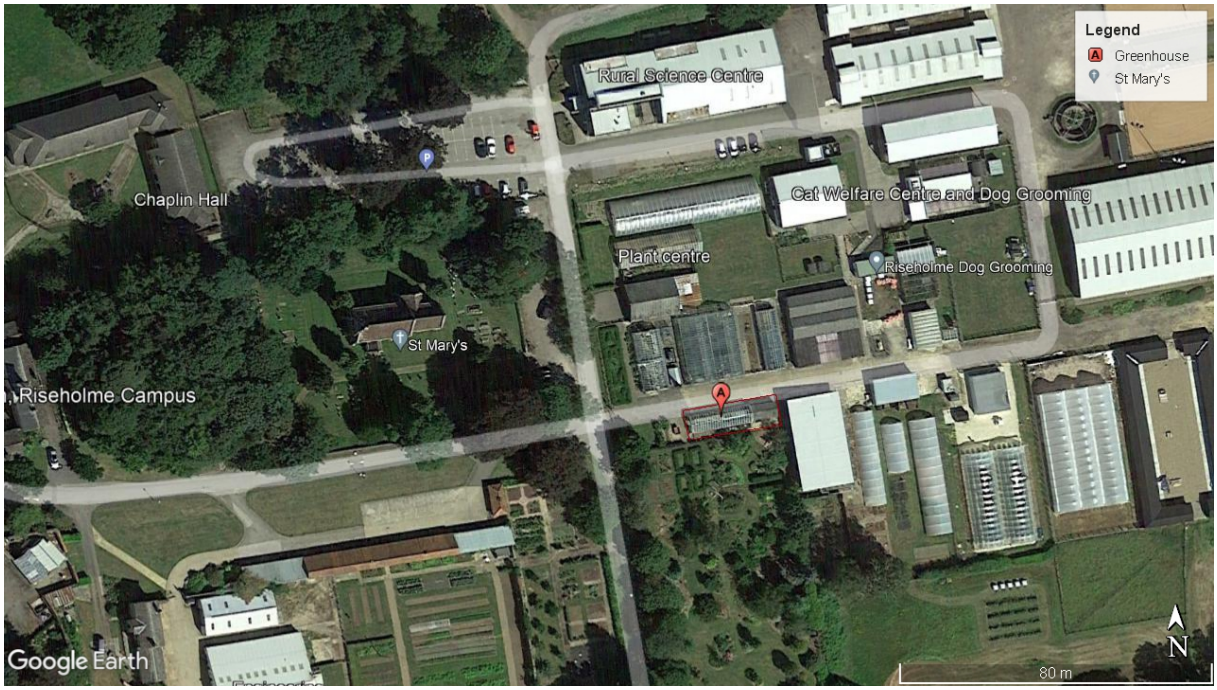

Figure 1: An aerial view of a portion of Riseholme Campus showing the position of the greenhouse (A).

Any modelling and data discussed relating to the solar thermal collector (STC) system are in reference to a small ($\pm$ 1.5m^2) collector installed at the south-east corner of the greenhouse although this system was not operational during the time in which data was collected. While this lack of results does not discourage the development of a theoretical model for the STC system, not enough data or design information is known about the technology currently being tested by ICaRE4Farms to produce a model of sufficient quality.

[1] 900kWh/m^2 vs. 350kWh/m^2 which is closer to a 260% efficiency increase.

[2] Figure 24 in the appendix shows the STC technology being tested although this particular installation is not used the thermally regulate a greenhouse.

[3] Nearby buildings on the site, such as Riseholme Hall and the accompanying stable block, also hold heritage status and so may have further fueled this issue.

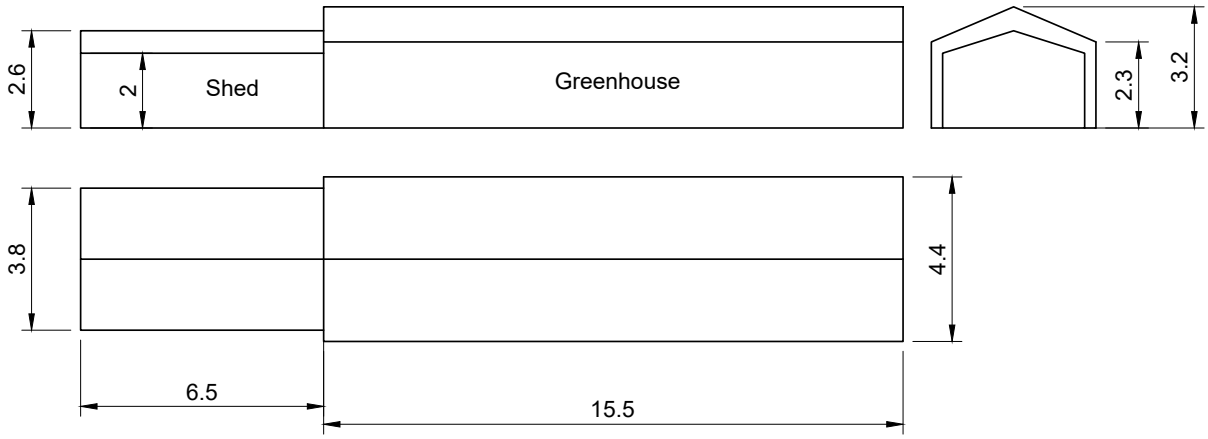

Figure 2: Dimensions of the greenhouse and attached shed.

In light of the issues mentioned, the aim of this report is to develop a model which, when given input data in the form of solar irradiance, external temperature, relative humidity, and wind speed, returns a predicted internal air temperature. This prediction is then compared to, and validated by, real-world measured results.

7 Literature Review

7.1 Introduction

Sustainability in agriculture continues to grow in importance [3], as a growing population increases food demand and puts pressure on increased supply efficiency. Climate change and urbanisation further push for the urgent need to adopt sustainable and effective agricultural solutions. Greenhouses offer a promising solution to help us meet the world's food needs, allowing for micro-climate control, alongside protection from weather events, pests, and diseases [3]. These benefits come at a cost, however, of a large energy consumption and great capital and labour investments. One of the main cost factors in commercial greenhouses is energy consumption, given that large amounts of energy are required to obtain high quality yields of a high quantity [4].

This is especially true for cold climates. These climates may greatly benefit from an increased agricultural output as this would reduce food transport costs and utilise non-arable space not otherwise able to be used for food production. These climates may not be ideal, however, due to unfavourable climate conditions increasing the energy required to meet minimum temperature and lighting requirements. Further energy requirements are needed for hot climates as well; areas too warm and dry to be arable may benefit from increased agricultural output using climate-controlled greenhouse solutions. The energy needed to heat 1m2 ranges from 500-2700MJ.m-2, depending on factors such as the site and the type of covering and climate control [5]. Reducing this energy consumption is also an important environmental consideration; oil and gas are traditionally used as a fuel source for heating systems in the greenhouse industry, negatively impacting the environment [6]. Interest in adapting alternative or renewable energy sources for heating to offset the relatively high price of these fossil fuels is currently high [7].

Carbon emission in the agricultural sector can be reduced through the strategic use of solar energy and thermal energy storage [3]. According to an Interreg market analysis, solar thermal energy (STE) has long been neglected in European countries due to climate conditions but is now an economical and renewable alternative to other energy sources such as oil, gas, and electricity [8]. Solar thermal collectors can be used to produce low enthalpy thermal energy for greenhouse heating systems. The collection and use of solar energy are especially attractive as greenhouses can considered to be a large solar collector. It would therefore be beneficial to focus our attention on increasing our understanding of STE solutions and to champion the adoption of STE technology within the agricultural industry.

7.2 Research Objectives and Motives

ICARE4FARMS is a research project funded by the Interreg North-West Europe Programme which aims to test the relevance and potential development of STE technology in North-Western European agriculture. This is to aid the EU's goal of increasing the share of renewable energy consumption which currently sits at 17%, and to reduce greenhouse gas emissions by 30%, a goal outlined by the Green Deal [8] [9]. The study aims to assess the current technical and financial conditions to estimate the development potential of STE systems as a replacement for conventional systems to heat water - a process which draws 40% of the energy consumed in farming in Northwest Europe [9]. Five main types of agricultural production have been identified as being potentially suitable for the adoption of STE [8]:

- Milk-fed calf farms that use hot water for feed production (reconstituted milk),
- Dairy farms and (particularly those that process milk on the farm),
- Pig farms, especially maternity and post-weaning units,
- Heated greenhouses: market gardening and horticulture,

- and Broiler poultry farms.

This research is concerned with heated greenhouses and addresses the practicality of using STE system to heat a hothouse, and to assess the real-world performance of the system by developing a digital model to investigate the dynamic energy behaviour of the installation.

A new solar thermal system is to be installed on a real-world greenhouse; the performance of this system is to be assessed – that is, how well this system maintains the hothouse within a bounded internal temperature range – and compared to mathematical model which defines the theoretical performance of the system. This mathematical model is to be created and implemented using MATLAB, wherein collected temperature data can be inputted to obtain a predicted internal hothouse temperature which can then be compared to the measured results. Other data such as weather conditions, solar irradiance, and physical system attributes (such as dimensionality and material thermal properties) are also required inputs of the model.

This research problem can be broken into constituents, all of which are well defined and understood in the current literature: the modelling of greenhouses, the modelling of solar-thermal collectors, the modelling of heat exchangers, and the modelling of systems in terms of higher-order dynamic energy transfer. The research and model proposed by this work is not novel in terms of the underlying understanding and theory of these constituents, but rather is novel in their specific application and combination.

7.3 Historical Background

There are three approaches that can be used to model greenhouses: static, intermediate, and dynamic models [10]. Static models approximate energy consumption from the total thermal gains and losses of the system. Solar energy is not considered, and meteorological data is supplied over large time steps (monthly or yearly). Whilst these models are comparatively simple, they lack precision, reporting $\pm 25\%$ error. This contrasts the $\pm 10\%$ error reported from dynamic models. These models show good precision in predicting both energy needs and interior climate. Three of these models were compared by Van Bavel et al. [11], with seven sets of data representing a large variety of input conditions. A disadvantage of this approach is a drastic increase in model complexity as well as a requirement for higher resolution input, within the range of hourly meteorological data. Intermediate models are not as complex or accurate as dynamic models as the neglect certain heat transfer modes but are more capable than simple statistical models. This research uses a dynamic model using algebraic and differential equations, albeit less in-depth than those produced by some other models.

According to a review presented by Sethi et al., the heat and mass balance inside a greenhouse are the most important requirements for a mathematical thermal model and in general, energy balance equations are listed as simultaneous first order differential equations [10]. The approach of this research follows this: to formulate a model using an energy balance approach to construct a series of differential equations to describe the system. These equations are also usually resultant of investigating the heat transfer modes and elements within the greenhouse. For the sake of simplicity, some of these transfer modes may be approximated or removed entirely, if their effect on the overall energy dynamics is small.

These equations can likely be combined to represent the system using state-space modelling. Many greenhouse models have been developed which utilise this methodology (see [12] and [13]). A disadvantage to this approach is the requirement for a "white box" understanding of the systems involved. This level of system understanding may not be possible in the face of information constraints on the technology used in this research, alongside time constraints. Furthermore, no controller design is required. For these reasons, state-space system modelling is not pursued in this research.

Once a dynamic or intermediate model has been constructed and once a series of equations are formed, the problem of how to solve them becomes apparent. Computer programs written

in languages such as C++ and MATLAB allow for system equations to be solved with great flexibility. However, when further complexity is required, pre-developed simulation programs may be used such as TRANSYS, HORTICERN, HORTITRANS, and MICGREEN [10]. Computational fluid dynamics (CFD) software may also be used for specific problem sets. These existing solutions allow for analysis to be completed without deriving and building a model from the ground up. Both of these numerical, computer-based approaches may use a variety of techniques – usually iterative – to solve the system equations such as Newton Raphson's technique, the Crank-Nicholson procedure, the Gauss-Seidel method (as used by Singh et. al. [14]), the finite difference method, etc.

Modelling the greenhouse system is only a part of the goal of this research; it is also necessary to consider the modelling of the heating system as a form of energy collection to be input into the greenhouse model. Both the greenhouse and the heating system are treated as coupled yet individual systems and so utilise their own distinct mathematical models. A variety of thermal models coupled with heating and heat storage systems are analysed by Sethi et al. [10].

A solar thermal collector, otherwise known as a hot water module, is simply some unit or device which collects heat by absorbing solar radiation [15]. They are the most critical components of any solar system [16]. These collectors are not only utilised for residential and commercial building heating but are also used in greenhouse-specific space heating [17] and drying [18] applications. There are different types of solar thermal collectors used in greenhouse applications, namely flat plate solar thermal collectors, concentrating soler thermal collectors, and evacuated tube solar collectors. The table below shows the different applications assigned to different solar collector variants [19].

Flat plate collectors are usually implemented to offset heating loads, rather than act as the primary source of heat generation [15]. Applications of these collectors are shown by Benli et. al. [17] as well as Attar et. al. [20]; in both instances, the flat plate collectors supplemented other heat storage and generation methods. They operate within a temperature range of 20-80 °C [21] as opposed to a range of 50-200 °C for evacuated tube solar collectors [22]. For higher heat requirements of 120-300 °C, concentrating solar collectors can be used [23]. Concentrating solar thermal collectors come in many types, mainly compound parabolic concentrators, parabolic trough collectors, linear Fresnel reflectors, and solar dish concentrators [24]. The Fresnel lens collector is attractive for use in greenhouse applications due to its low cost and high thermal efficiency [25] and are better than non-concentrating collectors in terms of efficiency, according to Sait et al. [26]. Due to their ability to deliver energy at high temperatures, concentrating thermal collectors can be considered more suitable for greenhouse heating [19].

The evacuated tube solar collector (ETSC) is another alternative which offers increased efficiency when compared to conventional flat plate collector designs, especially within the context of unfavourable environmental conditions such as cold and cloudy weather. Sabiha et al. report this collector to be the most efficient solar collector design, and they report a multitude of ETSC types, alongside their structure, applications, and challenges [27].

Anderson et al. successfully utilised the f-chart method – initially developed by Klein et al. [28] to characterise the long-term performance on solar heating systems – to analyse a solar thermal heating system for an aquaponics food production system [29]. This method was further utilised by Malquori et al. to evaluate the energy efficiency of various greenhouse shapes [30] as well as Rigby, A.R. as a design tool for the "Burnley Low Energy Greenhouse" [31]. Furthermore, Haberl et al. [32] reviewed the literature surrounding this method and found that the f-chart method agrees with measured data within a range of 2% to 15%. They report that this method can be used estimate the long-term average performance of multiple solar systems including water storage heating and building storage heating. The performance of flat-plate, evacuated tube, and compound parabolic concentrating solar collectors can all be evaluated using the f-chart method.

8 Model Description

8.1 Solar Radiation Considerations

Accurately describing the solar radiation is important to building a valid and suitable model. Of primary concern is calculating the incident solar radiation and its components: beam, diffuse, and reflected radiation on each surface of the greenhouse as well as the cover absorbance and transmittance.

A large part of the extraterrestrial solar radiation that strikes the earth is reflected back into space or absorbed or scattered by the atmosphere. The scattered radiation that reaches the surface of the earth is known as the *diffuse* radiation and that which makes it through the atmosphere directly is known as the *beam* or *direct* radiation. Figure 3 illustrates these concepts and more information can be found in *Solar Energy Engineering: Processes and Systems.* by Soteris A. Kalogirou [33].

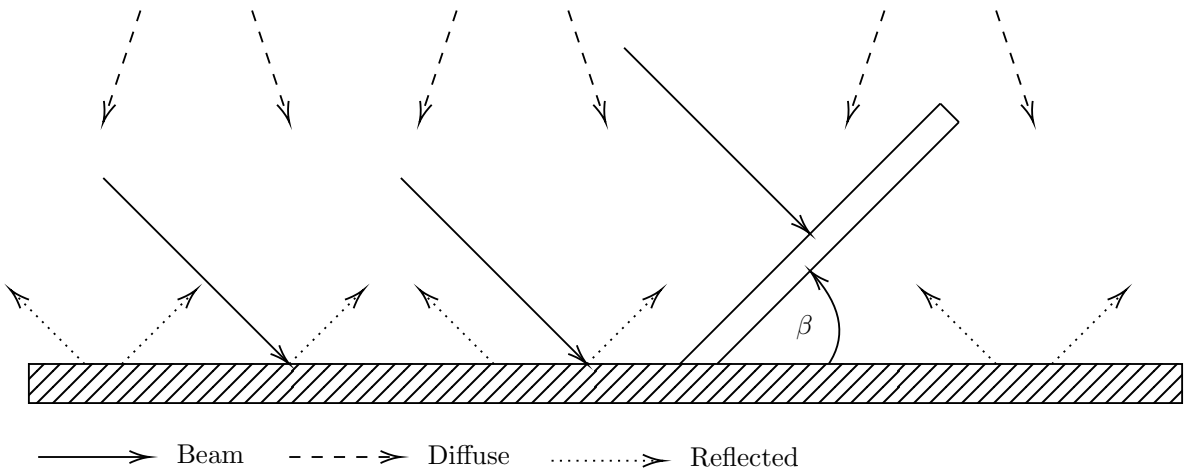

Figure 3: Various types of solar radiation with reference to an angled plane.

8.1.1 Solar Radiation on Various Surfaces

The solar radiation intensity on an inclined surface is estimated by the following equation, given by Duffie and Beckman [34]:

$$S(t) = I_b R_b + I_d R_d + (I_b + I_d)\rho R_r \tag{1}$$

Applying this to each surface element, i, and summing to obtain the total solar radiation incident on the cover, we obtain

$$S(t) = \sum_{i=1}^{6} = A_i \left(I_b R_{b(i)} + I_d R_{d(i)} + (I_b + I_d)\rho R_{r(i)} \right) \tag{2}$$

$$I_d = I_{dif} I_o \tag{3}$$

$$I_b = (1 - f_{dif}) I_o \tag{4}$$

The diffuse and beam radiation can be calculated by equations 3 and 4, where both I_d and I_b are the measure of intensity on a horizontal plane. f_{dif} is the fraction of diffuse radiation. A popular method of calculating this term is by using the Reindl correlation, as referenced by Boland et al. [35], which may be more suitable as data was sourced from "European and North American locations". Muneer et al. [36] compare a multitude of well-established correlations

and suggest their own single regression curve, shown in equation 5, by pooling data from 10 locations in the UK[4].

$$f_{dif} = 0.089\overline{k_t^2} - 1.185\overline{k_t} + 0.95 \tag{5}$$

the clearness index can be calculated by [37]

$$k_t = \frac{E_{global,measured}}{E_{clear}} \tag{6}$$

where E_{clear} is the clear sky irradiance, adapted from Bourges [38], given by

$$E_{clear} = 0.78 G_{on} \sin \gamma_s{}^{1.15} \tag{7}$$

where γ_s is the elevation of the sun and G_{on} is the extraterrestrial irradiance, given by Duffie and Beckman [39]

$$G_{on} = G_{sc}\left(1 + 0.033 \cos \frac{360n}{365}\right) \tag{8}$$

where G_{sc} is the solar constant and n is the day of the year. Note that a more accurate equation is given by Spencer (1971); see equation 1.4.1b from *Solar Engineering of Thermal Processes*.

Alternatively, Boland et al. [40] suggest the logistic function in equation 9, fitted to measured data with β_0 and β_1 acting as location-specific parameters; their values for Bracknell, England are -4.38 and 6.62 respectively. Bracknell is approximately 200km from the physical test site at Riseholme and suffers from greater light pollution with a SQM value[5] of 19.11 mag/arc sec^{-1} as opposed to 20.34 mag/arc sec^{-1}, according to the *lightpollutionmap*[6] website. Both of these factors may have a large effect on the accuracy of the results.

$$f_{diff} = \frac{1}{1 + e^{\beta_0 + \beta_1 k_t}} \tag{9}$$

For this equation, k_t is the hourly clearness index and is equal to I_{global}/G_{on}. Yet another method of calculating d_{dif} for equations 3 and 4 above is that cited by Zhang et al. [42] as being sourced from van Ooteghem et al. [43], which takes the form

$$f_{dif} = \begin{cases} \max(f_{dif1}, f_{dif2}) & \text{if} \quad \text{sun up} = 1 \\ 1 & \text{if} \quad \text{sun up} = 0 \end{cases} \tag{10}$$

where f_{dif1} and f_{dif2} are, respectively

$$f_{dif1} = \begin{cases} 1 & \text{if} \quad \tau_{atm} \leq P_{db} \\ 1 - P_{da}(\tau_{atm} - P_{db})^2 & \text{if} \quad P_{db} < \tau_{atm} \leq P_{dc} \\ 1 - P_{da}\left((\tau_{atm} - P_{db})^2 - (\tau_{atm} - P_{dc})^2\right) & \text{if} \quad \tau_{atm} > P_{dc} \end{cases} \tag{11}$$

$$f_{dif2} = P_{dd} + (1 - P_{dd})\left(1 - \exp\left(\frac{0.1}{\sin \beta}\right)\right) \tag{12}$$

P_{da}, P_{db}, P_{dc}, and P_{dd} are experimentally determined parameters and τ_{atm} is the atmospheric transmission value and is calculated using $\tau_{atm} = I_o \cos \theta_z / G_{on}$ where θ_z is the zenith angle.

[4]The areas and values used can be found in table 1 in the appendix.

[5]See *Sky Quality Meter measurements in a colour-changing world* by Sánchez et al. [41] for more information on this type of brightness measurement.

[6]www.lightpollutionmap.info

This last method for calculating f_{dif}, outlined in equation 10, was used to obtain the results in this report. Figure 17 in the results section shows the net radiation incident on the cover, calculated using equation 2. The view factors for the diffuse, beam, and reflected incident light components for each surface of the greenhouse can be calculated by using equations 13–15; a brief description of view factors is presented in section 8.2.2 below. β_i is the slope of surface i relative to the horizontal and θ_i is the angle of incidence for beam radiation with respect to surface i.

$$R_{d(i)} = \frac{1 + \cos\beta_i}{2} \tag{13}$$

$$R_{b(i)} = \frac{1 - \cos\beta_i}{2} \tag{14}$$

$$R_{r(i)} = \frac{\cos\theta_i}{\cos\theta_z} \tag{15}$$

8.1.2 Cover Absorbance and Transmittance

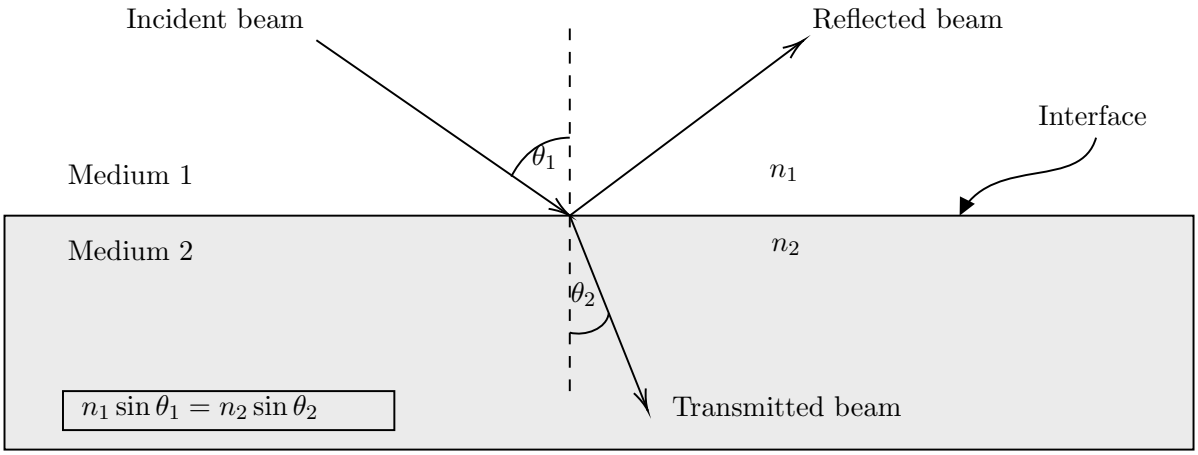

Figure 4: Angles of incidence, θ_1 and refraction, θ_2, following Snell's law.

It is important to investigate the transmittance and absorbance of the cover as a function of the incident angle, θ_1, to accurately calculate the radiation energy transferred to the cover as this angle changes with respect to time. Expressions for perpendicular ($\perp$) and parallel ($\parallel$) components of radiation for smooth surfaces were derived by Fresnel as [33]

$$r_\perp = \frac{\sin^2(\theta_2 - \theta_1)}{\sin^2(\theta_2 + \theta_1)} \tag{16}$$

$$r_\parallel = \frac{\tan^2(\theta_2 - \theta_1)}{\tan^2(\theta_2 + \theta_1)} \tag{17}$$

The overall reflection of the solar radiation with respect to some surface is the average of these perpendicular and parallel components:

$$r = \frac{1}{2}(r_\perp + r_\parallel) \tag{18}$$

The transmittance, reflectance, and absorptance of a single cover are given by equations 19, 21, and 22 respectively. Note that while these are given for the perpendicular radiation component, the same relations hold true for the parallel component; the subscript $\perp$ is simply to be replaced with $\parallel$.

$$\tau_\perp = \frac{\tau_\alpha(1 - r_\perp^2)}{1 - (r_\perp \tau_\alpha)^2} \tag{19}$$

where τ_α is the transmittance. The subscript α indicates that only absorption losses are considered. This can be calculated using

$$\tau_\alpha = \exp\left(\frac{-KL}{\cos\theta_2}\right) \tag{20}$$

where K is the extinction coefficient, which can very from 4m^{-1} to 32m^{-1} for high and low quality glass respectively [33]. L is the thickness of the glass.

$$\rho_\perp = r_\perp(1 + \tau_\alpha\tau_\perp) \tag{21}$$

$$\alpha_\perp = (1 - \tau_\alpha)\left(\frac{1 - r_\perp}{1 - r_\perp\tau_\alpha}\right) \tag{22}$$

As in equation 18, the overall transmittance and absorbance values of the cover are taken as the average of the perpendicular and parallel components:

$$\tau = \frac{1}{2}(\tau_\perp + \tau_\parallel) \tag{23}$$

$$\alpha = \frac{1}{2}(\alpha_\perp + \alpha_\parallel) \tag{24}$$

It can be seen that these are functions of the incidence angle, which is to be calculated for beam, diffuse, and reflected radiation for each surface. The incidence angle for each of these can be calculated by equations 25, 29, and 30 respectively. The beam angle, otherwise simply known as the solar incidence angle, is given by Duffie and Beckman [34] in equation 25 below.

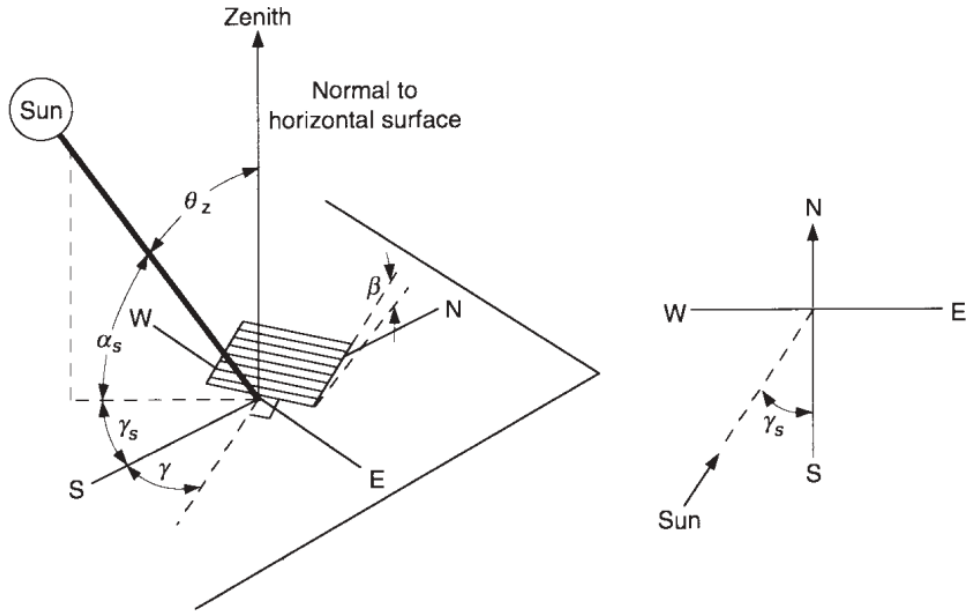

Figure 5: The notation used to describe the zenith angle, slope, surface azimuth angle, and solar azimuth angle for a tilted surface, courtesy of *Solar Engineering of Thermal Processes* by Duffie and Beckman [39].

$$\begin{aligned}\cos\theta = {} & \sin\delta\sin\phi\cos\beta - \sin\delta\cos\phi\sin\beta\cos\gamma \\ & + \cos\delta\cos\phi\cos\beta\cos\omega + \cos\delta\sin\phi\sin\beta\cos\gamma\cos\omega \\ & + \cos\delta\sin\beta\sin\gamma\sin\omega\end{aligned} \tag{25}$$

where δ can be found via

$$\delta = 23.45 \sin\left(360 \frac{284 + \text{daynr}}{365}\right) \tag{26}$$

where *daynr* is the number of day of the year. ω is the solar hour and θ_z is the zenith angle. Respectively, they can be calculated using

$$\omega = 15 \times (t - 12); \tag{27}$$

$$\theta_z = \cos^{-1}(\cos\phi \cos\delta \cos\omega + \sin\phi \sin\delta) \tag{28}$$

where t is the time in decimal form and ϕ is the location latitude. θ_d and θ_g below are equivalent angles of incidence for beam radiation that give the same transmittance and absorption values as diffuse radiation and ground reflected radiation respectively, and are expressed as

$$\theta_d = 59.7 - 0.1388\beta + 0.001497\beta^2 \tag{29}$$

$$\theta_g = 90 - 0.5788\beta + 0.002693\beta^2 \tag{30}$$

The transmittance and absorption values for diffuse, ground-reflected, and beam radiation can thus be calculated using equations 23 and 24.

The total solar irradiance transmitted into the greenhouse, I_{trans}, is given by

$$I_{trans} = \sum I_{trans(i)} A_{(i)} \tag{31}$$

for each surface i where

$$I_{trans(i)} = I_b R_{b(i)} \tau_{b(i)} + I_d R_{d(i)} \tau_{d(i)} + (I_b + I_d) \rho R_{r(i)} \tau_{g(i)} \tag{32}$$

Equation 31 therefore becomes:

$$I_{trans} = \sum_{i=1}^{6} A_{(i)} \left(I_b R_{b(i)} \tau_{b(i)} + I_d R_{d(i)} \tau_{d(i)} + (I_b + I_d) \rho R_{r(i)} \tau_{g(i)} \right) \tag{33}$$

Note that while the upper limit of $i = 6$ for the above sum refers to the 6 planes of the greenhouse (4 walls and 2 ceiling planes), this report only takes into account 5 surfaces on account of an attached shed replacing one of the walls.

8.2 Energy Balance for Various Components

8.2.1 Internal Air Component

The following equation is supplied by Zhang et al. [42] having been augmented slightly to include the Q_{h_a} and Q_{a_o} terms, and represents the energy balance for the interior air temperature. It is one of four simultaneous differential equations which make up part of their greenhouse model. Further simultaneous equations are supplied in section 8.4 of *Optimal Control of Greenhouse Cultivation* by van Straten et al. [44] although it is not always clear as to how strictly empirical these equations are.

The energy balance equation for the internal air is

$$\rho_a c_{p\_a} V_a \frac{\mathrm{d}T_a}{\mathrm{d}t} = -Q_{a\_f} - Q_{a\_c} + Q_{h\_a} - Q_{a\_o} + Q_{rd_a} \tag{34}$$

where ρ_a is the density of air which, for dry air, can be calculated as

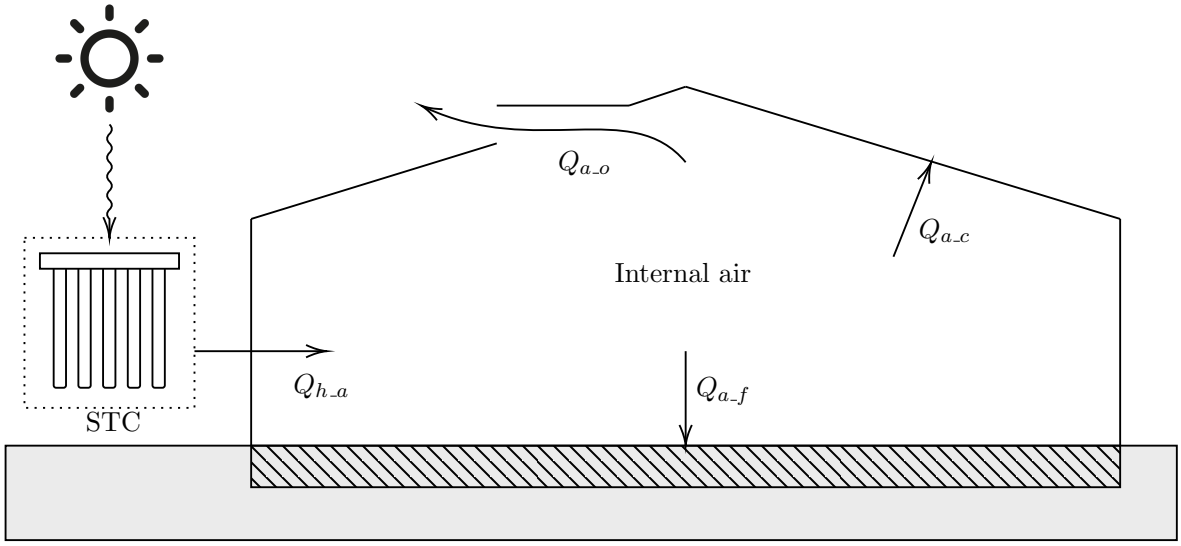

Figure 6: Heat transfer components considered for the internal air energy balance equation. *STC* refers to the solar thermal collector, expanded upon in section 8.4.

$$\rho = \frac{p}{R_{sp}T} \tag{35}$$

where p is the absolute pressure in Pa, T is the absolute temperature in K, and $R_{sp} = R/M_d$, where R is the universal gas constant and M_d is the molar mass of dry air.

It is expected that the air will be relatively humid, especially when taking into account the transpiration of the internal vegetation, and it is therefore more accurate to calculate the density using an equation offered by Shelquist [45] which has an error of less than 2% for $-10 < T < 50$ °C. Alternative equations exist to calculate the density as a function of pressure, humidity, and temperature. For now, ρ_a is assumed to be constant given that it doesn't deviate largely; it can be calculated via one of these alternative equations by using the recorded averages of the required parameters.

c_{p_a} is the heat capacity of the internal air which is itself a function of characteristic properties such as temperature and humidity. It can be simply and accurately expressed as an approximate empirical formula, as stated by Çengel et al. [46]

$$c_{p\_a} = 1.005 + 1.82H \tag{36}$$

where H is the absolute humidity which itself is a function of temperature and relative humidity and can be calculated using [47]

$$H = \frac{CP_w}{T} \tag{37}$$

where $C = 2.16679$ gK/J, T is the temperature in K, and P_w is the vapour pressure in Pa and can be calculated using the Antoine equation, which can be rewritten as:

$$P_w = 10^{A-B/(C+T)} \quad where \begin{cases} A & = 8.07131 \\ B & = 1730.63 \\ C & = 233.426 \end{cases} \quad for \quad 1 < T < 99°\text{C} \tag{38}$$

Alternative equations exist to calculate P_ω which sacrifice simplicity for higher degrees of accuracy such as the *Tetens equation* or *Buck equation* among others.

Alternatively, a simpler[7] approach is to employ the empirical relation below (equation 39) by Peter Mander [48], wherein the value of H can be calculated in terms temperature and relative humidity, rh in conjunction with equation 36.

$$H = \frac{6.112 \times rh \times 2.1674 \times \exp\left(\frac{17.67T}{T+243.5}\right)}{T + 273.15} \tag{39}$$

where T is in degrees Celsius and H is in g/m^3. Figure 23 in the appendix shows this relationship for a finite set of temperature values at all possible rh values.

Referring back to equation 34, V_a is simply the volume of internal air and T_a is the temperature. Q_{a_f} is the heat transfer from the air to the floor, and is defined by equation 64 in section 8.2.3 below and Q_{a_c} is the heat transfer from the air to the cover, given by

$$Q_{a\_c} = A_c \alpha_{a\_c}(T_a - T_c) \tag{40}$$

where A_c is the area of the cover and α_{a_c} is the coefficient of heat transfer from the air to the inside of the cover, given as

$$\alpha_{a\_c} = 3|T_a - T_c|^{1/3} \tag{41}$$

Q_{a_o} is the ventilation heat loss and is calculated by considering the number of air changes per hour, N_a, which can be expressed as [49]

$$N_a = \frac{\dot{m}_a(3600)}{V_a \rho_a} \tag{42}$$

where $\dot{m}_a$ is the mass of air that has moved out of the building per second. Given $Q = cm\Delta t$ and rearranging equation 42 for $\dot{m}_a$, Q_{a_o} can be described as

$$Q_{a\_o} = \frac{c_{p\_a} N_a V_a \rho_a (T_a - T_o)}{3600} \tag{43}$$

where T_o is the exterior air temperature. An alternative ventilation heat exchange term is offered by Du et al. [50]:

$$Q_{ven} = Q_{a\_o} = V_{ven}(\rho_a c_{p\_a} + h_{fg}\epsilon)(T_o - T_a) \tag{44}$$

where V_{ven} is the volumetric ventilation rate (m^3/s), h_{fg} is the latent heat of vaporization of water (J/kg), and ϵ is the exchange coefficient between temperature and humidity (kg/(m3 °C)). Note that this final term is not necessary if the density of air has already been adjusted based on its humidity content. Finally, Q_{h_a} is the energy added by the solar thermal heater. By placing this term wholly in the internal air energy balance equation, it is assumed that the heat exchanger does not directly add any energy to the floor or the cover. The expression for this term (see equation 69) as well as other calculations regarding the solar thermal system can be found in section 8.4 below. Finally, Q_{rd_a} is the heat absorbed by the internal air, and is simply given by

$$Q_{rd\_a} = \eta_{rd\_a} I_{trans} \tag{45}$$

where η_{rd_a} is stated to be 0.05.

[7] Not the *simplest* approach; one may, if accuracy is of lesser concern, refer to pre-calculated tables such as that offered by Dr Israel Urieli, available at
https://www.ohio.edu/mechanical/thermo/property_tables/air/air_Cp_Cv.html

8.2.2 Cover Component

Some papers simply assume the cover temperature to be the average of the external and internal air temperatures. A more accurate temperature can be calculated from the following cover energy balance relation [44]

$$\rho_c c_{p\_c} V_c \frac{\mathrm{d}T_c}{\mathrm{d}t} = Q_{rd\_c} + Q_{f\_c} + Q_{a\_c} - Q_{c\_o} - Q_{c\_sk} \tag{46}$$

Note that the energy transfer from the cover to the crop has been removed for the sake of simplicity. The word *cover* refers, in this case, to the glass of the greenhouse, although other materials may be used by changing the equation parameters. Figure 7 shows the heat transfer elements stated in equation 46.

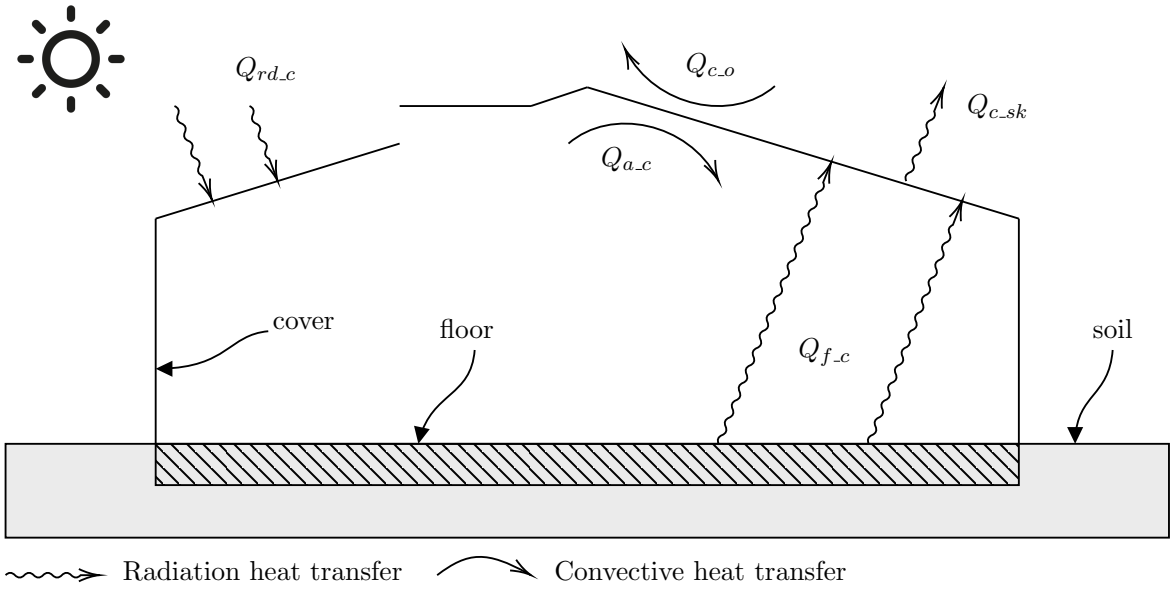

Figure 7: Heat transfer components considered for the cover energy balance equation.

The equation for Q_{rd_c} is given by van Ooteghem [43]:

$$Q_{rd\_c} = \eta_{rd\_c} A_c I_c \tag{47}$$

where η_{rd_c} is the absorption coefficient (1 − albedo) and is stated by Taki et al. to be 0.0173 [51]. This is different for the glass used at Riseholme campus, of course.

Q_{f_c} is the radiation heat transfer from the floor surface to the cover and is given as

$$Q_{f\_c} = A_f E_f E_c F_{f\_c} \sigma \left(T_f^4 - T_c^4 \right) \tag{48}$$

where A_f is the area of the floor surface (uncovered), E_f and E_c are the emission coefficients of the floor and cover respectively, and F_{f_c} is the view factor between the floor and the cover. T_f and T_c are in degrees K.

The convection heat transferred from the internal air to the cover, Q_{a_c} is given by equation 40 and the convection heat transferred from the cover to the external air is given by

$$Q_{c\_o} = A_c \alpha_{c\_o} (T_c - T_o) \tag{49}$$

where α_{c_o} is an empirical function of the outdoor wind speed, v_o [44]:

$$\alpha_{c\_o} = \begin{cases} 2 + 1.2v_o & \text{if} \quad v_o < 4 \\ 2v_o^{0.8} & \text{if} \quad v_o \geq 4 \end{cases} \tag{50}$$

Alternatively, many other equations exist to calculate the convective heat coefficient as a function of wind speed, some of which are plotted in figure 8. Mirsadeghi et al. [52] explored and compared a range of these formulae, taking into account experimental derivation and other dependent factors such as surface orientation.

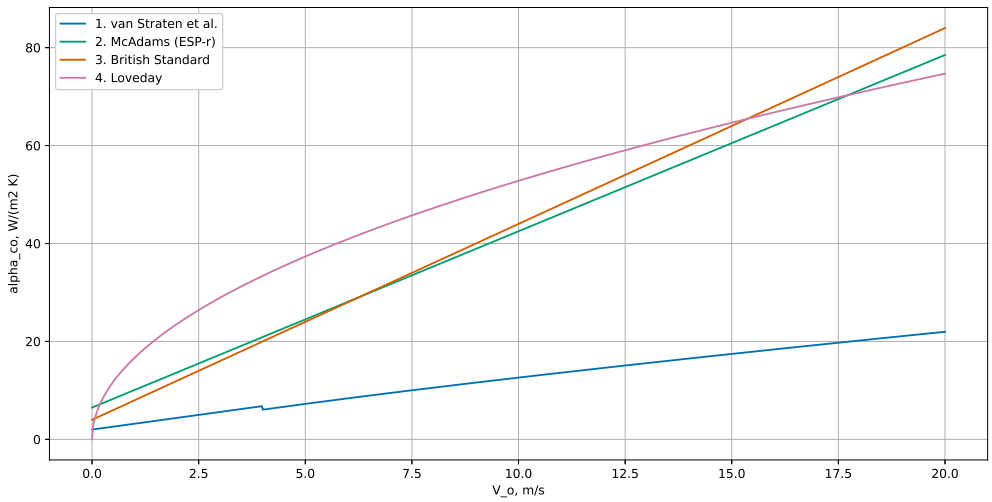

Figure 8: Some empirical convective heat coefficient formulae. (1) courtesy of van Straten et al. [44], (2, 3, 4) courtesy of Mirsadeghi et al. [52]. It can be seen that equation 50 deviates noticeably from some of the others presented in the literature.

Lastly, Q_{c_sk} is the long-wave radiation heat transfer from the cover to the sky, and is calculated as

$$Q_{c\_sk} = A_c E_c E_{sk} F_{c\_sk} \sigma \left(T_c^4 - T_{sky}^4 \right) \tag{51}$$

where

$$T_{sky} = 0.0552 (T_o)^{1.5} \tag{52}$$

as proposed by Swinbank [53]. Note that the temperature terms in equations 51 and 52 are in K. Furthermore, F_{c_sk} is the view factor in the direction from the outdoor side of the greenhouse cover to the sky. Given two surfaces located arbitrarily in space, the view factor is the portion of radiative heat flux that leaves one surface and strikes another [54]. It is a purely geometrical parameter and is a scalar value between 0 and 1. A variety of methods can be used to calculate its value[8], many of which are used in conjunction with finite element methods.

Many empirical equations exist which can be used to calculate the effective sky emissivity; of the 9 different correlations referenced by Gliah et al. [57], the following given by Berger et al. [58] is a simple function of the dew point temperature, T_d:

$$E_{sk} = 0.77 + 0.0038 T_d \tag{53}$$

[8] such as Double Area Integration, the Monte Carlo and the hemi-cube method [55], Nusselt Sphere, the Crossed-Strings method and others [56].

where T_d can be calculated using the following equation, given by Lawrence [59], although more complex equations can be used to obtain a greater degree of accuracy. T_d is in °C and rh is a percentage value.

$$T_d = \frac{100 - rh}{5} \tag{54}$$

8.2.3 Floor and Soil Component

The energy balance equation for the floor (the components of which are shown in figure 9 below) is given by

$$\rho_f c_{p\_f} V_f \frac{\mathrm{d}T_f}{\mathrm{d}t} = Q_{s\_f} - Q_{f\_a} + Q_{rd\_f} \tag{55}$$

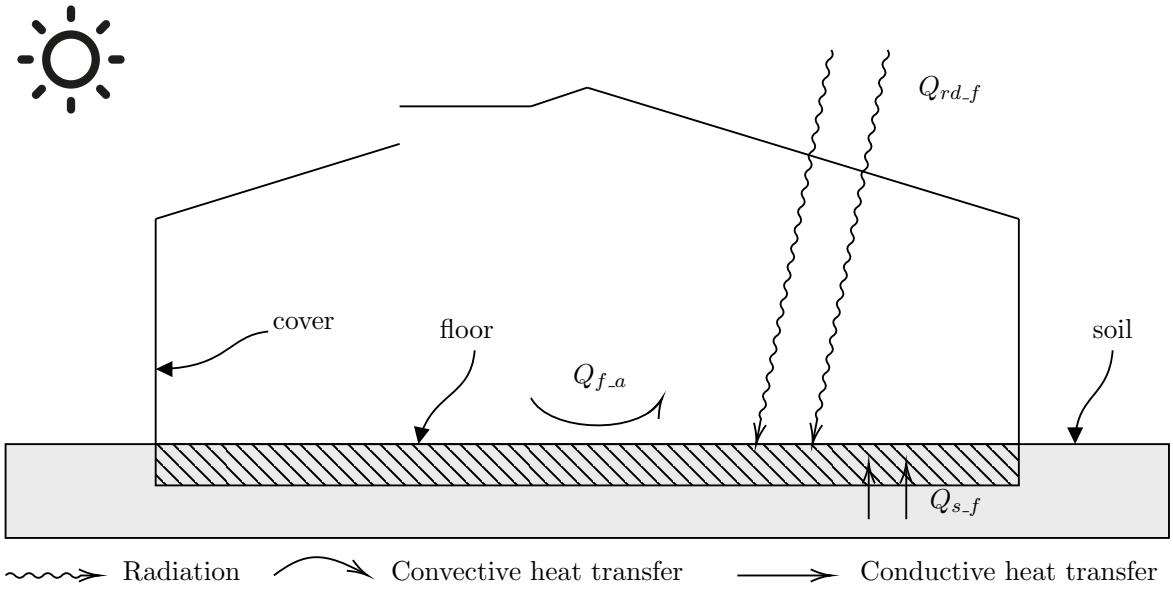

Figure 9: Heat transfer components accounted for for the floor energy balance equation.

Q_{f_a} describes the heat transfer from the floor to the internal air; it is modelled as natural convection and assumes a negligible internal air velocity.

$$Q_{f\_a} = h_f A_f (T_f - T_a) \tag{56}$$

where h_f is the convective heat transfer coefficient and is expected to fall within the range of 2.5-25 W/m^{2}K for air under free (non-forced) convection, according to table 12.2 from *Exploring Engineering* by Koski et al. [60]. While usually determined experimentally, it can be calculated by the following relation [61]:

$$h_f = \frac{Nu \cdot k_a (2W + 2L)}{A_f} \tag{57}$$

where k_a is the thermal conductivity of air, which can be calculated by an empirical function of the absolute temperature, T, given by the U.S. Standard Atmosphere, 1976 [62] as

$$k_a = \frac{2.64638 \times 10^{-3} \cdot T^{3/2}}{T + 245.4 \times 10^{-12/T}} \tag{58}$$

This formula shows good agreement with the tabulated data given by Çengel and Cimbala [63] at a pressure of 1 atmosphere. Nu, for the upper surface of a horizontal plate, has been experimentally determined to follow the relation given by

$$Nu = \begin{cases} 0.54Ra^{1/4} & 10^4 < Ra < 10^7 \\ 0.15Ra^{1/3} & 10^7 < Ra < 10^{11} \end{cases} \tag{59}$$

Ra is the Rayleigh number, a dimensionless quantity defined below as a product of the Grashof and Prandtl numbers. According to Zeneli et al., it determines whether buoyancy-driven natural convection plays an important role in heat transfer [64].

$$Ra = GrPr = \frac{g\beta(T_f - T_a)\delta^3}{\nu^2} \cdot Pr \tag{60}$$

where β is the coefficient of volume expansion (otherwise known as volume exapansivity); this property represents the variation of the density of a fluid with temperature at constant pressure. Assuming that the internal air can be modelled as an *ideal gas*, β can be calculated as the inverse of the absolute temperature: $\beta = 1/T_a$. ν is the kinematic viscosity of the fluid, defined as the ratio of absolute (dynamic) viscosity to density, $\nu = \mu/\rho$. Absolute viscosity (kg/m.s) can be represented as a function of temperature only, as shown in equation 61 below [62]. While pressure does have an effect on this value, it is considered independent on viscosity for low to moderate pressures (in the range of a few percent to several atmospheres) and so does not need to be considered for cases in which pressures deviate only slightly from standard atmospheric values [63].

$$\mu = \frac{\beta_\mu T^{3/2}}{T + S} \tag{61}$$

where $\beta_\mu = 1.458 \times 10^{-6}$ and S is the Sunderland's constant, equal to 110.4K. The kinematic viscosity can therefore be obtained by combining the results of equations 61 and 35. Alternatively, an empirical equation for ν as a function of T can be obtained if the density, ρ of air is assumed to be a function of T only, with the absolute pressure assumed to be constant. δ in equation 60 refers to the characteristic length of geometry (m) which, for an isothermal horizontal plate, is A_f/p_f where p_f is the perimeter of the floor.

The Prandtl number of the air, Pr, can be considered a constant at $Pr = 0.73$ although to calculate the number exactly, the following formula is used:

$$Pr = \frac{\mu c_{p_a}}{k_a} \tag{62}$$

It may be simpler, however, to obtain Pr from a linear fit of known tabulated data [63] given the low error observed (approximately 0.2%), given by

$$Pr = -0.000234T_a + 0.735 \tag{63}$$

subject to $-40°\text{C} \leq T \leq 60°\text{C}$ where T_a is the temperature in degrees Celsius.

Q_{s_f} is the conductive heat transfer from the soil to the floor (assumed to be a uniform homogeneous concrete slab), and is given by

$$Q_{s\_f} = k_f A_f (T_f - T_s) \tag{64}$$

It is assumed that, for damaged concrete, $k_f = 1.74\text{W/mK}$ [65]. Kim et al. [66] found that the factors with the largest influence on the thermal conductivity of concrete are the aggregate volume fraction and the moisture condition, based off experimental data. Regrettably, these values are not known for the experimental setup at Riseholme. Asadi et al. [67] present a review of the conductivity of concrete, linking to research outlining commonly used techniques for measuring thermal conductivity and its influencing factors as well as suggesting an exponential fit to estimate the thermal conductivity given density:

$$k_f = 0.0625e^{0.0015\rho} \tag{65}$$

While the slab is a 3D object and the thermal conduction equations need to consider this, it can be simplified to a 2D problem with the heat flow contributed by the soil on at the sides being considered negligible. s_f is the thickness of the floor slab.

Q_{rd_f} is the energy transferred into the floor via incident solar radiation, and can be expressed as

$$Q_{rd\_f} = (A_f - A_{pl})\eta_f I_{trans} \tag{66}$$

The radiation energy incident on the floor is assumed to only be sourced from that transmitted through the cover; no other elements are taken into account as interacting with the floor via radiative heat transfer due to their relatively small contribution with respect to the solar radiation incident on the greenhouse. η_f is the shortwave absorption coefficient of concrete, assumed to be 0.6 [68] and I_{trans} is the solar irradiance transmitted through the cover as given in equation 31, incident on the floor of the greenhouse. A_{pl} is the area taken up by the plant-covered tables. Re-phrasing this area in terms of the proportion of floor-space, x, taken up by the tables, then Q_{rd_d} can be rewritten as

$$Q_{rd\_f} = (1 - x)A_f\eta_f I_{trans} \quad x \leq 1 \tag{67}$$

8.3 Attached Shed

The greenhouse has attached to it a shed at one end, used to house potting supplies and store miscellaneous equipment. While there is an internal door to partition this space off from the rest of the greenhouse, the internal air in this shed is assumed to mix freely and sufficiently with the rest of the air in the greenhouse such that the air can be considered homogeneous and of uniform temperature between these two spaces. Any energy added or removed from this space via conductive heat exchange with the outside environment is therefore assumed to effect the temperature in the greenhouse as much as in the shed and vice versa.

The conductive heat exchange of the shed and the environment, Q_{sh} can be calculated by:

$$Q_{sh} = \sum \frac{k_i A_i \Delta T}{d_i} \tag{68}$$

where k_i, A_i, and d_i are the conductive heat coefficient, area, and thickness of each building element; only the walls and roof elements are considered for which the characteristics are assumed or approximated. The shed's ventilation heat transfer as well external incident solar radiation effects are considered negligible.

8.4 Solar Thermal System

The heat transfer into the internal air can simply be modelled as

$$Q_{h\_a} = \mu I_{he} A \tag{69}$$

where μ is the overall efficiency of the solar thermal collector and heat exchanger systems and I_{he} is the solar radiation incident on the collector which can be calculated using equation 1.

8.4.1 Heat Exchanger

The heat exchanger used consists of a series of pipes running through the greenhouse which are exposed to the internal air. The efficiency of this system is dependent on many factors such as the flow rate of the fluid, pipe dimensions and properties, layout and installation, etc. At

the time of writing this report, the system is not installed and not enough details are known to make a model to sufficiently predict the efficiency of this system. It is therefore assumed that the effect of the heat exchanger and its efficiency is negligible.

8.4.2 Collector

The efficiency of the collector can be calculated given the following equation sourced from Duffie and Beckman [39].

$$\eta = \eta_0 - \frac{a_1 \Delta T}{I} - \frac{a_2 \Delta T^2}{I} \tag{70}$$

These parameters can be found on the Solar Keymark Certificate[9] for the model installed on the site. Figure 10 graphically shows this relationship and compares this performance with that stated in literature by Grahovac et al. [69]. ΔT is the difference between the fluid temperature and the ambient temperature ($T_{fluid} - T_o$). To account for the angle of the sun, we introduce a new parameter: the incidence angle modifier[10], K_θ which corrects for the tilt of the collector assuming incident beam radiation is not normal to it's surface. The incidence angle is measured from both longitudinal and transversal directions, represented by $K_{\theta L}$ and $K_{\theta T}$ respectively, each at a multitude of angles of 0° through to 90° [70]. The individual incidence angle modifier is simply the product of these two values:

$$K_\theta = K_{\theta L} \times K_{\theta T} \tag{71}$$

$K_{\theta L}$ and $K_{\theta T}$ are known and are shown in table 2 in the appendix, alongside a graph of K_θ as a function of the angle, shown in figure 25. The efficiency equation therefore becomes:

$$\eta = \eta_0 K_\theta - \frac{a_1 \Delta T}{I} - \frac{a_2 \Delta T^2}{I} \tag{72}$$

The optical collector gains are therefore [69]

$$Q_o = \eta_0 K_\theta I A \tag{73}$$

and the thermal losses are defined as

$$Q_{tl} = A\left(a_1(\Delta T) - a_2(\Delta T)^2\right) \tag{74}$$

The useful gains, therefore, is the difference between these values:

$$Q_u = \begin{cases} Q_o - Q_{tl} & Q_o > Q_{tl} \\ 0 & Q_o < Q_{tl} \end{cases} \tag{75}$$

9 Solving the Model

9.1 Data Processing

The various sources of data[11] used do not share the same time intervals; environment input data have intervals of 30m with measured internal temperature and humidity data having 5m intervals. It was therefore necessary to linearly interpolate the former, thereby equalising the data and assuring a smaller step size when solving the ODEs, which results in greater accuracy.

[9] The document is available online at http://www.duurzaamloket.nl/DBF/PDF_Downloads/DS_1703.pdf

[10] This is commonly denoted as IAM but given the usage of I and A in the immediate context, K_θ will be used to avoid confusion.

[11] Expanded on in section 10 below.

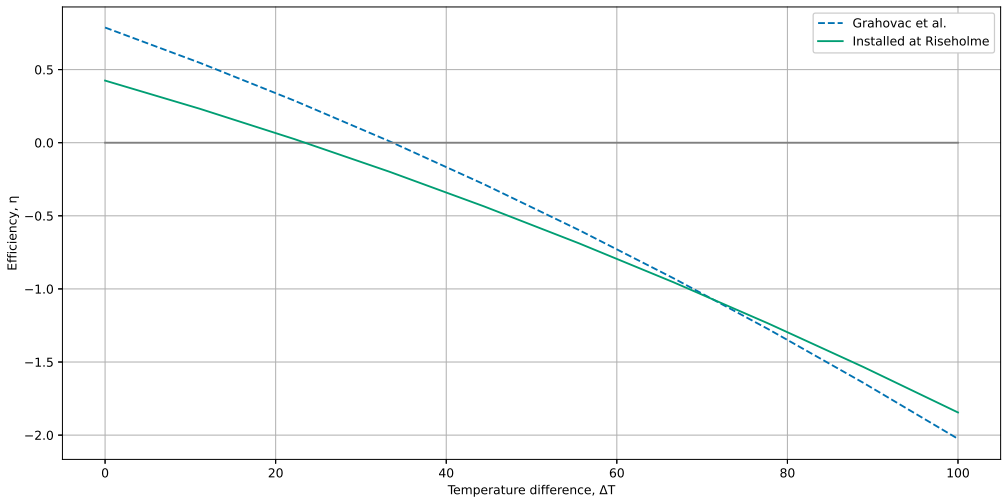

Figure 10: Comparison between collector efficiency and temperature difference. For both instances, the area was assumed to be 2.3m^2 and the solar irradiance was assumed to be 100Wm^{-2} [71].

9.2 Solving the Model

Many methods exist to solve ordinary differential equations (ODEs). The standard solver for ODEs in MATLAB is the `ode45` function. It implements a Runge-Kutta method to solve problems of the form[12]

$$\frac{\mathrm{d}x}{\mathrm{d}t} = f(t, x), \quad x(t_0) = x_0 \tag{76}$$

The finite difference method was initially employed but the afore-mentioned Runge-Kutta method was chosen due to a greater accuracy, as illustrated in figure 11. The accuracy of the solution is inversely proportional to the time step which is limited by the resolution of the measured data acting as the model input. In practice, it has been found to be difficult to implement the `ode45` function with sparse, discrete data. The data is therefore linearly interpolated using the built-in function `interp1` to return values for non-integer values of t. Listing 1 below is an abstracted version of the MATLAB code and shows the structure of this code used to solve the various energy balance equations. The full code used to obtain the results in this report is shown in listing 3 in the appendix.

```
% specify initial conditions; y0 & t0 vectors
Y0 = [initVal1 initVal2 initVal3];
t0 = [0 0 0];

% call ode45 solver
f = @(t, dYdt) ODEEqns(t, dYdt(1), dYdt(2), dYdt(3), inputData);
[t, dYdt] = ode45(f, tspan, Y0);
plot(t, dYdt(IndexOfValueToBePlotted));

function dYdt = ODEEqns(t, val1, val2, val3, inputData)

```

[12] This extends to a system of differential equations which take the form $\begin{pmatrix} y_1' \\ y_2' \\ \vdots \\ y_n' \end{pmatrix} = \begin{pmatrix} f_1(t, y_1, y_2, \ldots, y_n) \\ f_2(t, y_1, y_2, \ldots, y_n) \\ \vdots \\ f_n(t, y_1, y_2, \ldots, y_n) \end{pmatrix}$.

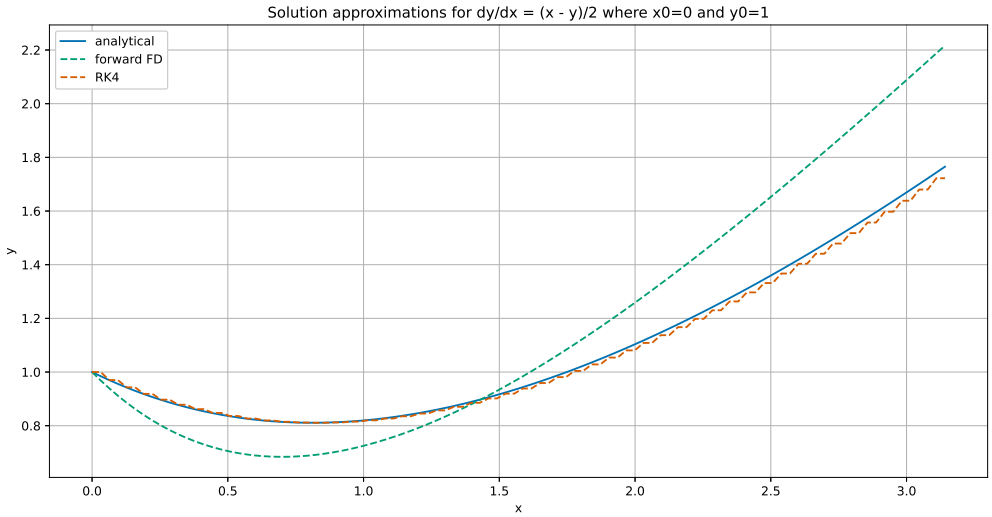

Figure 11: Comparison of RK4 and Forward Finite Difference methods against the analytical solution to an arbitrary ODE function.

```
% equations as functions of shared values and input data
dVal1dt = someFunctionOf(Val1, Val2, Val3, inputData); % energy balance eqn. 1
dVal2dt = someFunctionOf(Val1, Val2, Val3, inputData); % energy balance eqn. 2
dVal3dt = someFunctionOf(Val1, Val2, Val3, inputData); % energy balance eqn. 3

% output matrix
dYdt = [dT_adt; dT_cdt; dT_fdt];
end
```

Code Listing 1: `ode45` MATLAB code structure used.

10 Data Collection

To collect the internal air temperature data, two data loggers (Elitech HC-51[13]) were placed in the positions shown in figure 10 wherein the placement of a humidity sensor (Elitech RC-4HC[14]) is shown. Both sensors offer an accuracy of 0.5°C for $-20°C < T < 40°C$. The data are measured in 5 minute intervals with values from both temperature sensors averaged.

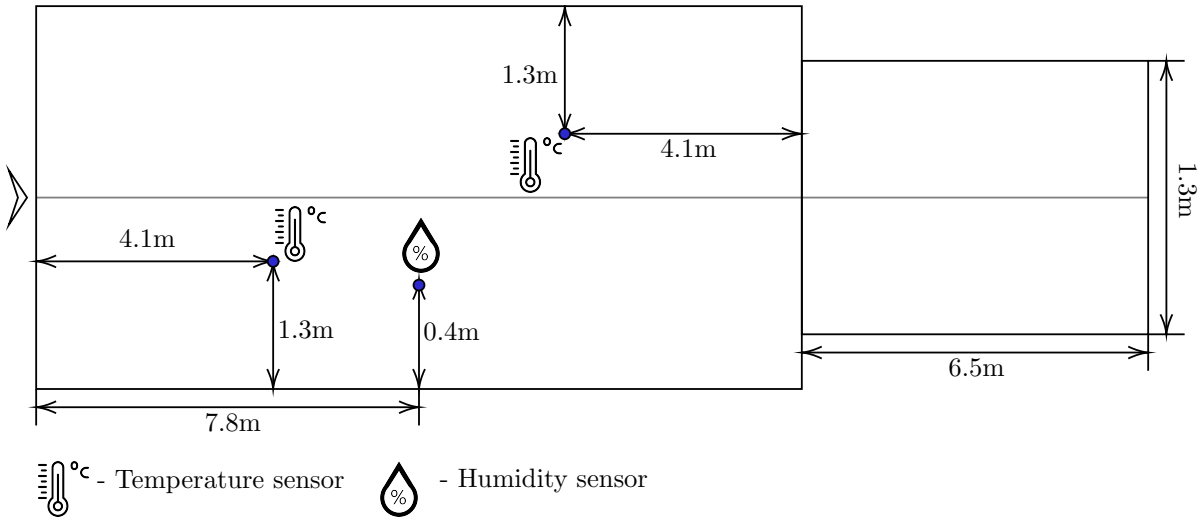

Figure 12: Location of the sensors within the greenhouse. The heights of the sensors are not taken into account. Diagram not drawn to scale.

In order to correct for measurement inaccuracies introduced by solar radiation incident on the temperature sensors, novel heat shields were fabricated. Botero-Valencia et al. [72] presented a drastic decrease in both temperature and humidity measurement error through the use of a 3D-printed solar radiation cover design; while the design used in this work does not follow theirs, it is still expected to have a significant role in reducing data error. The sensor itself is at the base of the logger and so the cover mainly acts as a radiation shield and a means of protecting the sensor from water or dripping condensation. Figure 13 shows the design used, with images of the real-word implementation shown in figure 26 in the appendix. The logger was assumed to be cylindrical and the exact design dimensions are not shown as they were defined arbitrarily, given that a thorough design process of the cover would not be time-efficient when considering other project deadlines and time constraints.

White PLA was used to 3D-print the cover with an infill of 40%.

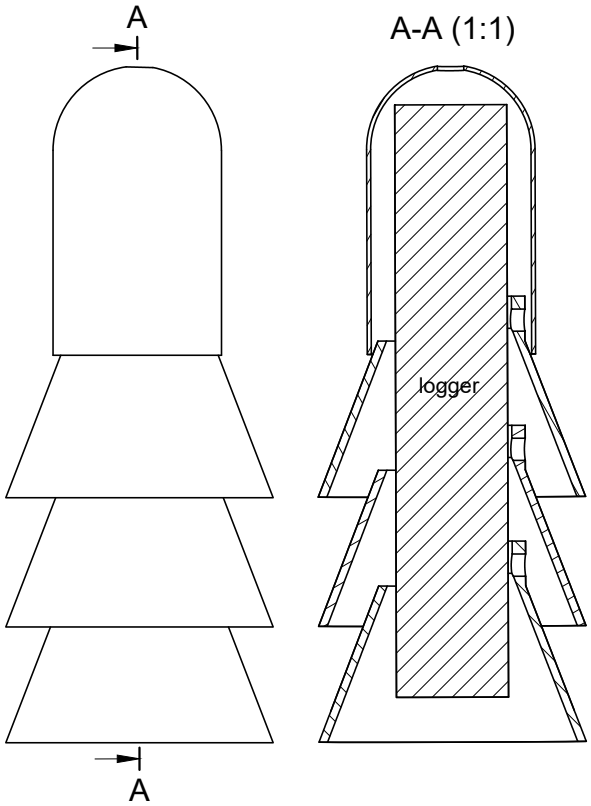

Figure 13: Technical drawing displaying the cross-section of the logger cover design used.

[13]Manual available at https://www.elitechlog.com/wp-content/manuals/rc-51-instructions.pdf
[14]Manual available at
https://www.elitechlog.com/wp-content/manuals/RC-4-RC-4HA-RC-4HC-instructions.pdf

Figure 10 below shows the recorded internal temperature and the status of agreement between the different data loggers. The disagreement between the loggers is greatest when the temperature is highest, suggesting that this is a result of direct radiation skewing the results; as contrasted by good agreement on cooler days when diffuse radiation is more prevalent.

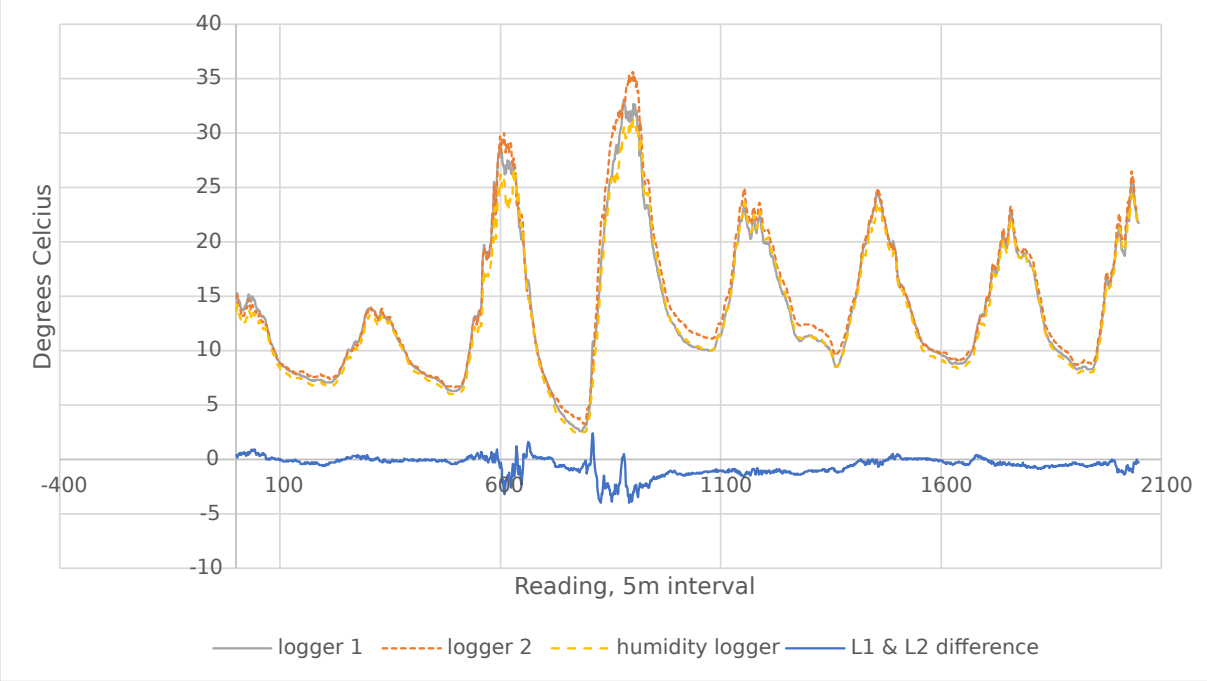

Figure 14: Recorded internal temperature measurements.

figure 15 below shows the relative humidity recorded. Figure 26 in the appendix shows the logger installed.

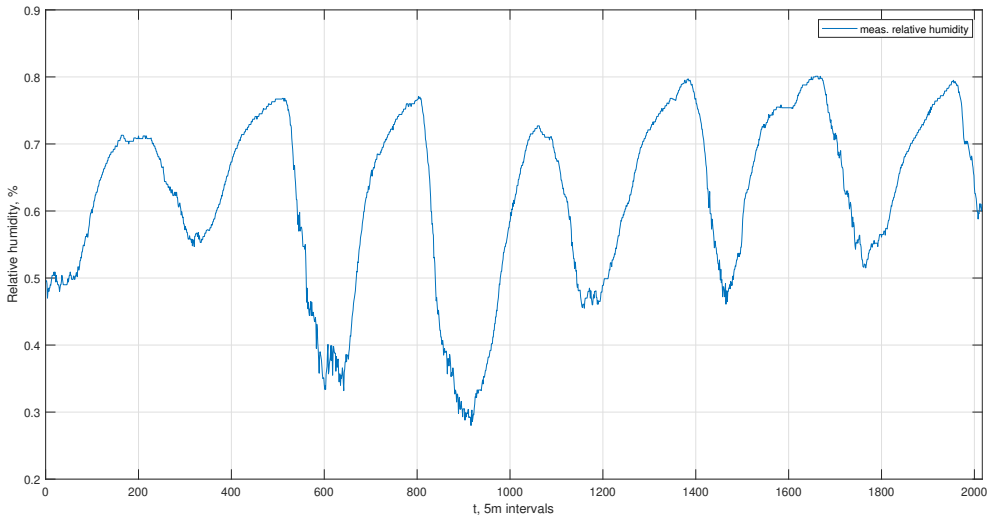

Figure 15: The measured relative humidity within the greenhouse.

The other data data required as model inputs (wind speed, external temperature, soil temperature, and solar radiation) we sourced from a COSMOS-UK site[15] about 0.8km south of the

[15]Part of the Cosmic-ray soil moisture monitoring network managed by The UK Centre for Ecology & Hydrology.

greenhouse at Riseholme as shown in figure 10. The highest resolution data available comes in 30m intervals; although this does not coincide with the 5 minute intervals captured by the internal temperature loggers, the long term scope of the temperature prediction should allow for linearly interpolating between the data points with little resulting error. The soil temperature data is available at a multitude of depths; for the soil temperature model input, T_s, data corresponding to a depth of 10cm was used given that the thickness of the concrete floor of the greenhouse is assumed to be between 5 and 10 centimetres.

Figure 16: The relative placement of the COSMOS-UK weather station (B) relative to the greenhouse (A) and the rest of the Riseholme Campus.

For more information about the network and the data it provides, see https://cosmos.ceh.ac.uk/

11 Results

11.1 Results

The total solar radiation incident on all faces of the greenhouse is shown in figure 17 below. The code used to obtain these results is shown in listing 2 in the appendix.

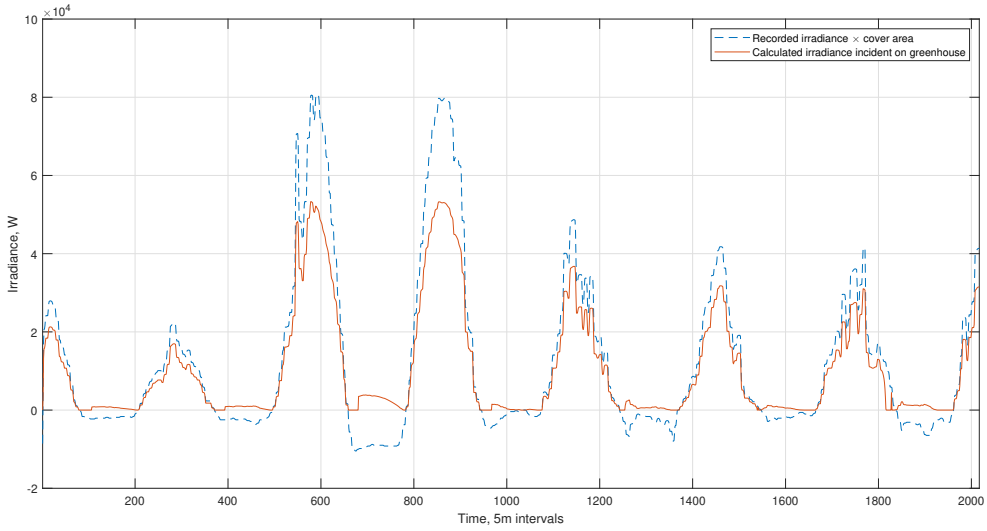

Figure 17: The calculated solar irradiance incident on the greenhouse cover. The based measured solar irradiance has been multiplied by the area, thereby normalising the two data sets and allowing for direct comparison.

Figure 18 below shows the predicted internal temperature, T_a. It is very similar to the external temperature, T_o, albeit with a minor decrease in amplitude as well as a lateral shift to the right, suggesting a higher thermal inertia. The rate of change of temperature is not nearly as high as $T_{a,\text{meas.}}$ which suggests either an underestimation of heat flowing into the internal air, or an overestimation of the denominator in the energy balance equation. The individual heat flow terms can be seen in figures 20 and 21.

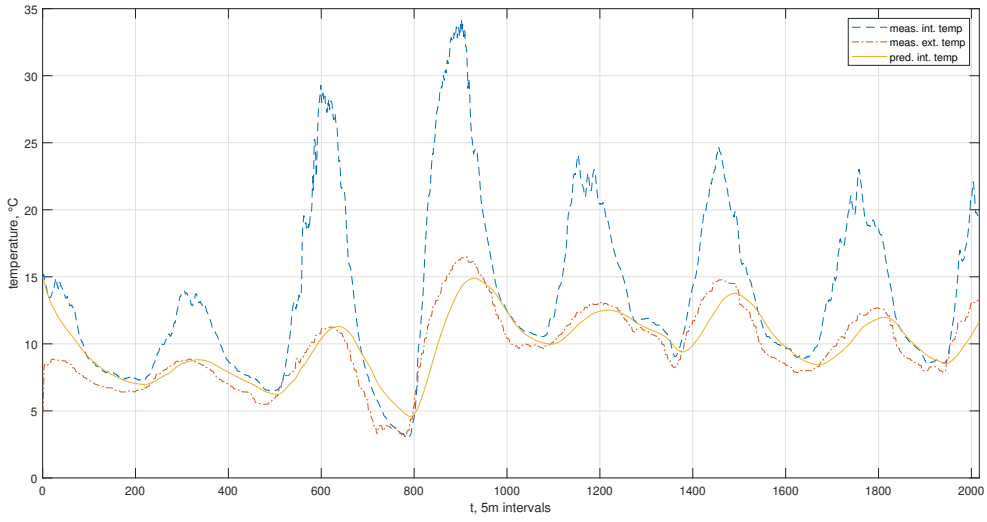

Figure 18: The model output prediction of T_a alongside the measured internal and external temperatures.

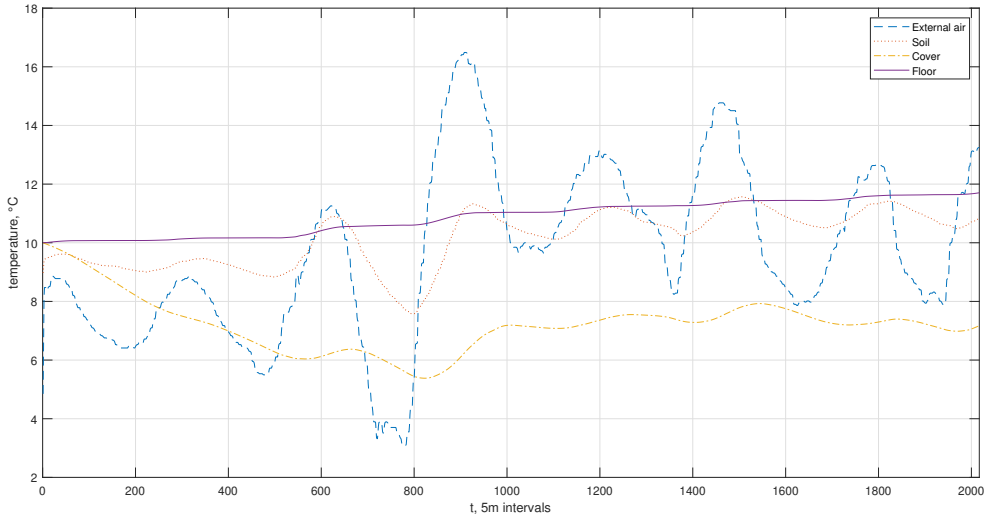

Figure 19: Temperature predictions for T_s, T_c, and T_f.

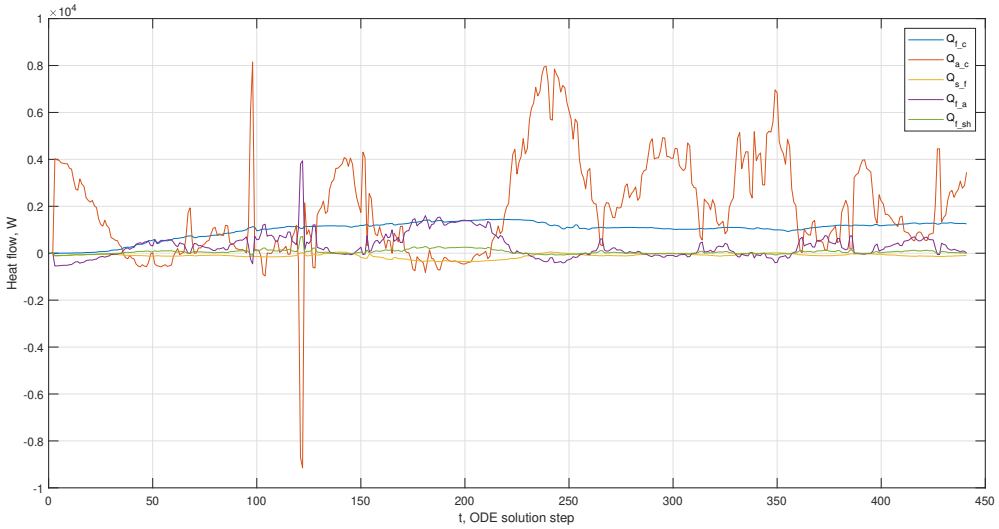

Figure 20: The solutions to each of the heat flow terms that are shared amongst two or more of the energy balance equations.

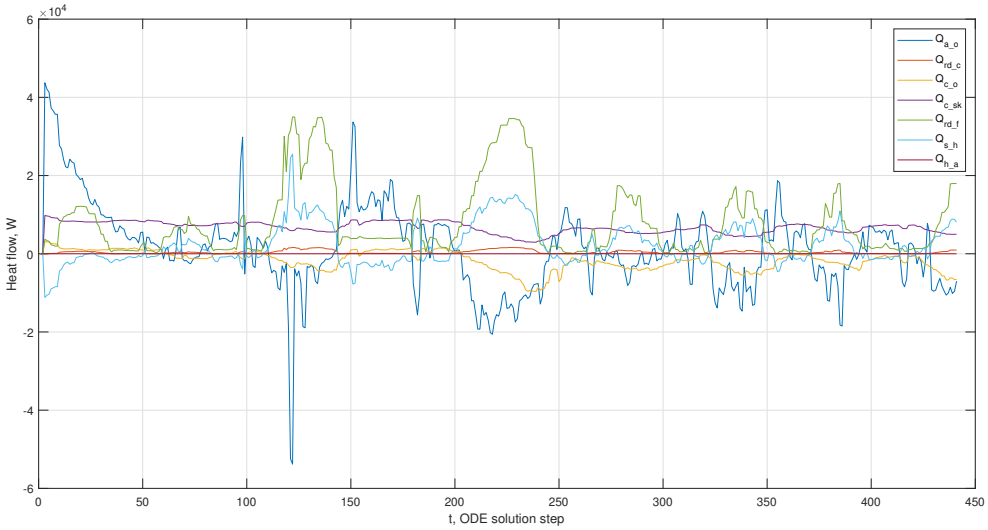

Figure 21: The solutions to each of the heat flow terms which only exist in one of the energy balance equations.

11.2 Error Evaluation

Two common methods of evaluating predictive error are *root mean square error* (RMSE) and *mean absolute error* (MAE), both of which are regularly employed in model evaluation studies according to Chai et al. [73]. Willmott et al. [74] state that MAE is unambiguous and is a more natural measure of average error as RMSE "is a function of 3 characteristics of a set of errors, rather than of one (the average error)". Chai et al. countered this, stating that RMSE is not ambiguous and is more representative of model performance when the error is expected to follow a Gaussian distribution. Since the error distribution cannot be confidently assumed to be unbiased[16] for the model presented in this paper, MAE will be used as the defining informative metric. However, for the sake of convention and the ability to directly compare performance between external papers and methods presented in literature, RMSE will be also be calculated.

MAE and RMSE are, respectively, defined as [73]

$$\text{MAE} = \frac{1}{n}\sum_{i=1}^{n}|e_i| \tag{77}$$

$$\text{RMSE} = \sqrt{\frac{1}{n}\sum_{i=1}^{n}e_i^2} \tag{78}$$

where $|e_i|$ is the absolute error at point i subject to $i = (1, 2, \ldots, n)$. The MAE, RMSE, and absolute error are shown in figure 22 below.

[16] A requirement when assumed to follow a normal distribution which itself is an underlying assumption in the usage of RMSE.

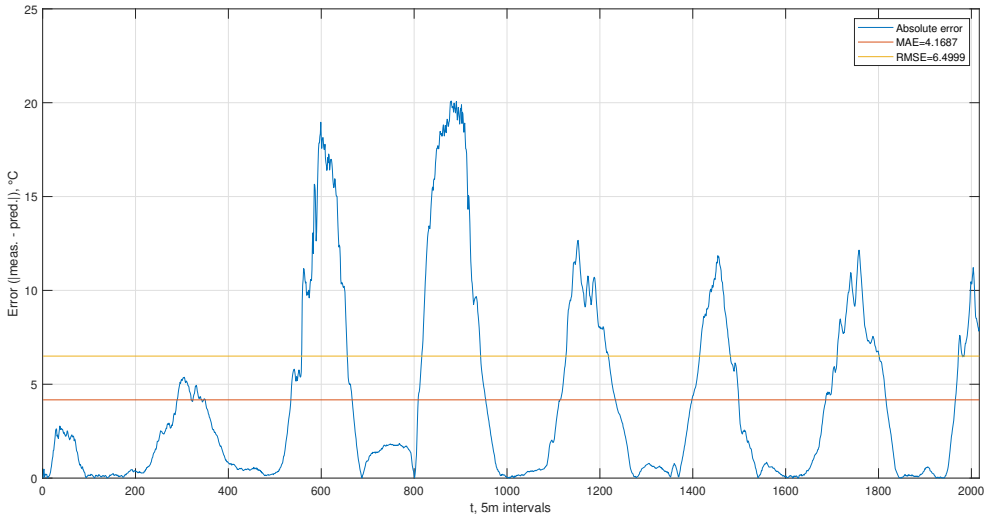

Figure 22: Various measures of model error.

12 Discussion

12.1 Reflection on Results

The results are not conclusive in their current form; while many of the model components work as expected, it is clear that various amendments need to be made in order for the model to perform sufficiently. While the MAE value is only 4°C, the cyclic nature of the error means that its maximum value is 20°C; such discrepancies lead to few use cases for the low-confidence output data.

Figures 20 and 21 show that the heat flow terms are widely varied in magnitude with significant spikes at places, and that the flow of heat happens in the correct direction for all terms. Q_{a_o} has the greatest value although it is not clear as to which has the greatest influence.

Referring to figure 19, it can be seen that the temperature of the soil has little short-term effect on the temperature of the floor. Furthermore the cover is almost consistently lower than the outdoor temperature which is to be expected due to the relatively large effect of the Q_{c_a} term.

12.2 Reflection on the Process

A multitude of revisions can be made to the model as well as the solving process. While not strictly necessary, the model can be made more accurate although many of these changes may offer minuscule improvements, potentially falling within the bounds of data measurement error. The main way to increase accuracy is to prune the numerous assumptions made and discard the simplicity they offer. Fewer assumptions about the attached shed would be beneficial alongside implementing more concrete values for the various measurements and thermal properties of the various components making up the greenhouse. Namely, the experimentally determined input parameters as well as the lack of radiation dynamics from the surrounding environment and the assumed *air changes per hour* value[17] may not be valid and likely contribute significant headwinds to the model's performance.

While the solar radiation calculations have been successfully implemented, it would likely be easier and more accurate, given the location of the greenhouse relative to surrounding buildings, trees, and other environmental features, to simulate the radiation dynamics using an appropriate software package. The solar irradiance incident on the floor and various cover surfaces would then be imported into the model as a function of time. Alternatively, real-world sensors could be used to collect this data although this is likely a less optimal choice as point sources of data would be extrapolated to represent that of the whole surface. Furthermore, this added complexity would increase cost and introduce potential points of failure.

The source of the environmental data is also an important factor and while the inconsistency in the time intervals likely had a small effect of the efficacy of the results, better-aligned data offering coinciding measurement intervals would have been desirable alongside having sensors placed closer to the greenhouse.

Finally, the soil temperature data was recorded at an uncovered site and so may fluctuate more than that present under the floor of the greenhouse; in the way it's currently implemented, it acts as a perfect heat sink as its temperature is not at all influenced by the temperature of the greenhouse floor. In this case, a multi-layer soil model would be beneficial. Furthermore, the addition of a plant community model component would be advantageous; heat flow terms relating to the crop were not implemented despite the greenhouse at Riseholme containing many plants which undoubtedly had an effect on its dynamic thermal behaviour.

[17] Calculating natural ventilation is a complex function of external and internal environmental factors as well as greenhouse geometry. The value used in this report follows no calculation procedure and is estimated and assumed constant. Kittas et al. [75] present methodology for calculating the volume flow rate between the inside and outside air of a greenhouse and how it is affected by temperature and wind effects. This methodology was successfully implemented by Singh et al. [76].

Large improvements can be made to the implementation of the MATLAB code and the solving process. Referring to listing 3, the `real()` function is used to isolate the real component of the results returned by `ode45` solver. These complex irregularities are only present in a portion of the results' column vectors and the i component appears to propagate over time. While the exact source of this error is not yet known, it is likely caused by terms which take the form x^n where n is a non-integer; if x ever becomes negative, this will result in complex numbers. Other terms such as those including logarithms may offer the same problem. Another culprit may be the adaptive time stepping used by the `ode` family of functions.

12.3 Improvements and Future Research

A large improvement to the process presented in this report would be to obtain better data[18] and to record the transient temperatures of the various modelled components such as the cover and the floor temperature. This would offer useful comparisons and troubleshooting information and allow the model to be validated for all three of the differential energy balance equations.

Another improvement would be to undergo a process of calibration and validation when constructing the model; a process successfully implemented by Singh et al. [76]. This would allow for the adjustment of experimentally determined input parameters to improve model performance without altering any methodology.

As mentioned in section 12.2 above, the assumption that the plant community within the greenhouse have a negligible effect undoubtedly had a negative impact on the performance of the model. Singh et al. [76] provides a model which places emphasis on the internal plant community when investigating the transient thermal behaviour of a naturally ventilated greenhouse when growing cucumbers; these elements provided in their model may be of use to improve the model presented in this report. Finally, the issues encountered when solving the model using MATLAB may be avoided by using another software package or even by migrating the model to SIMULINK, in which alternative ODE solvers are available for use.

12.4 Conclusion

Given the current predicted data, the model cannot be validated. However, in light of the issues observed with the practical implementation of the model discussed above, it cannot be conclusively stated as to whether its theoretical construction has a significant part to play in its under-performance. Further investigation is required into constructing an error-free solving environment and future efforts should be made to aggregate higher quality input data.

[18] Better location, with environmental data being recorded at the site of the greenhouse, as well as and better timing, with all data being collected synchronously and at matching time intervals.

13 Appendix

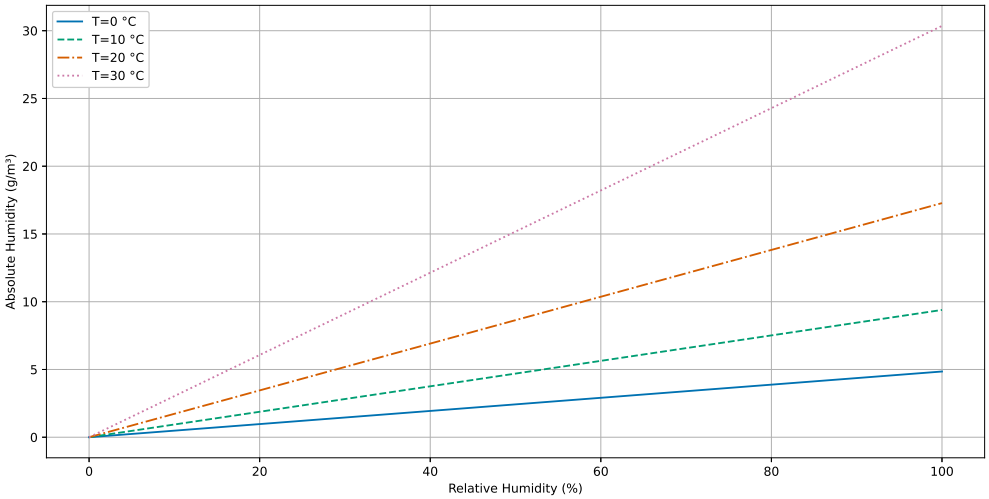

Figure 23: H as a function of the temperature and relative humidity.

Table 1: Annual ratio of diffuse to global radiation for various locations.

Location	Annual Ratio of Diffuse to Global Radiation
Jersey	0.51
Easthampstead	0.59
London	0.58
Aberporth	0.56
Cambridge	0.6
Aldergrove	0.61
Eskdalemuir	0.61
Lerwick	0.63

Figure 24: ICaRE4Farms STC installation, courtesy of the ICaRE4Farms LinkedIn page [1]

Table 2: K_θ for angles 0° through to 90°.

	10°	20°	30°	40°	50°	60°	70°	80°	90°
$K_{\theta L}$	1	1	0.98	0.96	0.91	0.82	0.68	0.43	0
$K_{\theta T}$	1.06	1.12	1.18	1.33	1.49	1.11	0.74	0.37	0
K_θ	1.06	1.12	1.16	1.28	1.36	0.91	0.50	0.16	0.00

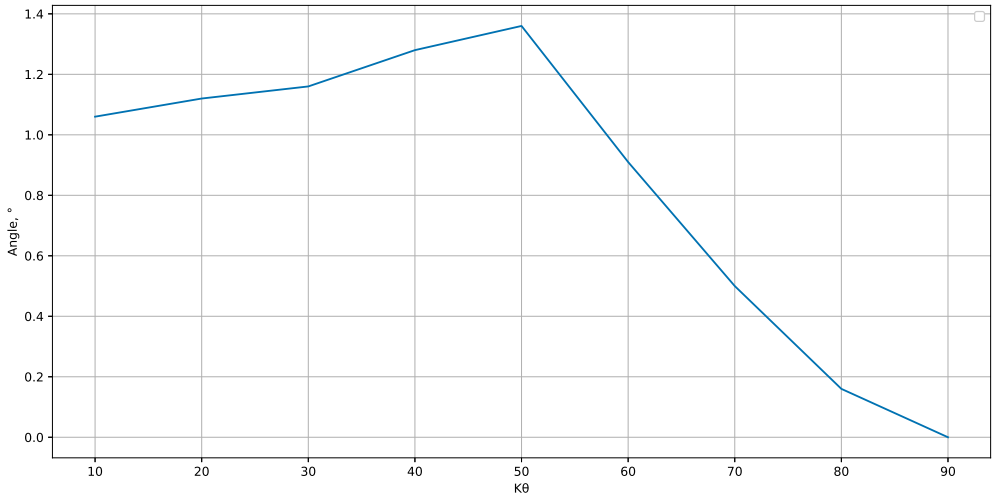

Figure 25: K_θ as a function of the angle.

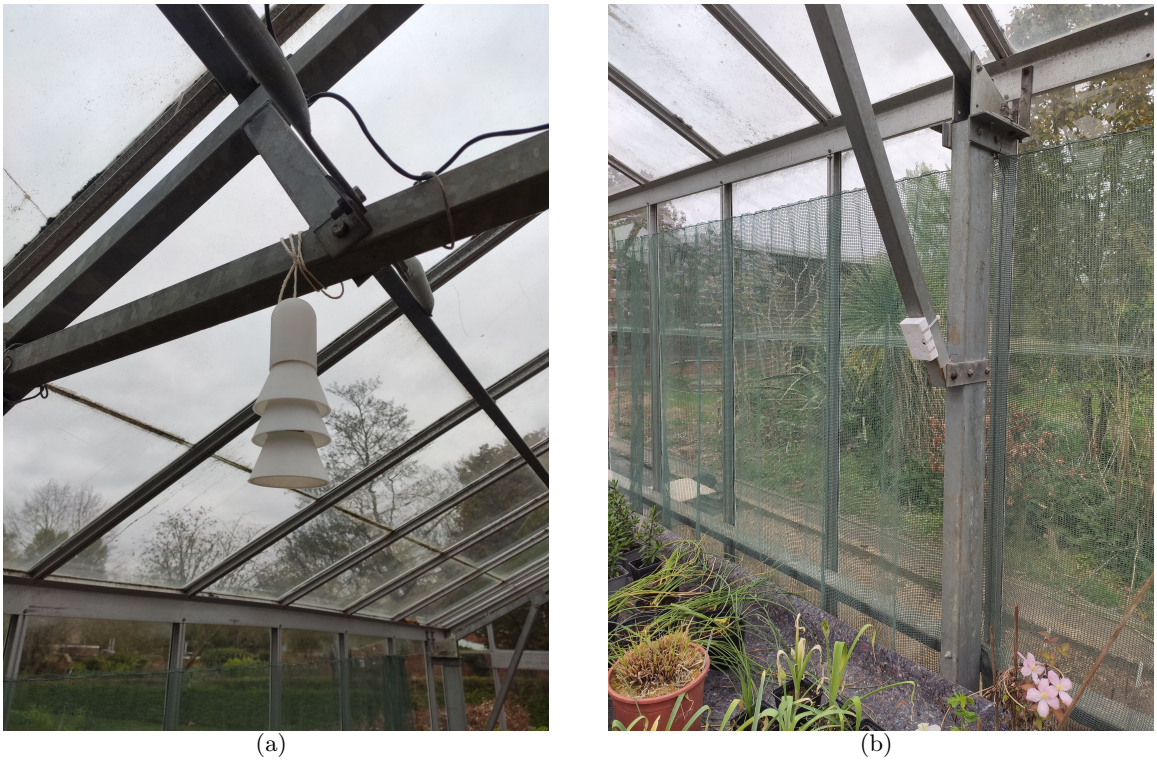

(a) (b)

Figure 26: Installation of (a) temperature logger and (b) humidity logger. While incident radiation on the humidity sensor was of lesser concern, the sensor remained in a cardboard box in which holes were cut to allow for air exchange.

(a) (b)

Figure 27: The back (a) and side (b) of the attached shed. The presence of the door is assumed to have a negligible effect.

(a) (b)

Figure 28: (a) The ventilation mechanism on the roof of the greenhouse. The hatch is open approximately 40cm and runs approximately the full length of the roof. It is unknown as to whether this hatch was closed, either partially of fully, throughout the data measurement process. (b) The greenhouse has multiple broken or missing panes, resulting in further ventilation heat losses.

Figure 29: Map displaying the Parish of Riseholme, centered about the grade II* heritage listed Parish Church of St Mary [77].

```
% solar calcs test
clear; delete 'rad.xlsx'
omega = readmatrix('hourAngle.csv');
zenith = readmatrix('zenith2.xlsx');
sunup = readmatrix('sunup.xlsx');
I_o = abs(readmatrix('IrrRecorded.csv')');
% t = 1:2017;
rad = ones(1, 2017);
for i = 1:2017
    rad(i) = calcRadiation(i, omega, zenith, I_o(i), sunup);
end
plot(I_o.*157); hold on
plot(rad); hold off; legend('Irr rec', 'rad calc')
writematrix(rad',rad.xlsx');

function x = calcRadiation(t, omegaInp, zenithInp, I_o, sunup)

    zenith = zenithInp(t);
    beta = [90 90 90 30 30]; %placeholder, order d l u ru rd when looking from
    above facing north
    azimuths = [170 -100 -10 -10 170]; % greenhouse rotated by about 10 degrees
    anti-clockwise
    areas = [35.65 12.1 35.65 36.74 36.74];
    daynr = 121; % 1st = middle day
    decl = 23.45*sind((360*pi*284*daynr)/(180*365));
    lat = 53.27;
    omega = omegaInp(t); % import data; solar hour, create w/ excel+python to
    extrapolate
    incidenceAngle = acosd(sind(decl).*sind(lat).*cosd(beta) - ...
        sind(decl).*cosd(lat).*sind(beta).*cosd(azimuths) + ...
        cosd(decl).*cosd(lat).*cosd(beta).*cosd(omega) + ...
        cosd(decl).*sind(lat).*sind(beta).*cosd(azimuths).*cosd(omega) + ...
        cosd(decl).*sind(beta).*sind(azimuths).*sind(omega));
    R_b = cosd(incidenceAngle)./cosd(zenith);
    R_r = (1 - cosd(beta))./2;
    R_d = (1 + cosd(beta))./2;

    G_sc = 1357; % (value used by NASA), see 28 of duffie and beckman
    G_on = G_sc*(1+0.033*cosd((360*pi*daynr)/(180*365)));
    tau_atm = I_o/G_on/cosd(zenith);

    pda = 6.4;
    pdb = 0.22;
    pdc = 0.4; % not known
    pdd = 0.2; % not known

    f_dif2 = pdd + (1-pdd)*(1-exp(0.1./sind(beta)));

    if tau_atm <= pdb
        f_dif1 = 1;
    elseif (tau_atm > pdb) & (tau_atm <= pdc)
        f_dif1 = 1 - pda*(tau_atm-pdb).^2;
    else
        f_dif1 = 1 - pda*((tau_atm-pdb).^2 - (tau_atm-pdc).^2);
    end

    if sunup(t) == 1
        f_dif = max(f_dif1, f_dif2);
    else
        f_dif = 0;
    end

    I_d = f_dif*I_o;
```

```
    I_b = (1-f_dif)*I_o;

    IrrSurfaces = I_b.*R_b + I_d.*R_d + (I_b+I_d).*0.2.*R_r;

    x = sum(IrrSurfaces.*areas); % 'return' statement
    if x < 0
        x = 0;
    end
end
```

Code Listing 2: The MATLAB code used to obtain the total solar radiation incident on all surfaces of the greenhouse.

```
% (c) James Philbrick, University of Lincoln, April 2022
% Applying Greenhouse thermodynamic predictive model to real-world data.

clear; clc; clearvars; close all;

nDataPoints = 2017;

% input data
T_o = readmatrix('externalTempRecorded.csv')';
T_s = readmatrix('soilTempRecorded.csv')';
Irr = readmatrix('rad.xlsx');
T_aRec = readmatrix('internalTempRecorded.csv');
windSpeed = readmatrix('windSpeedRecorded.csv')';
rh = readmatrix('relHumidityRecorded.csv')';
floorRad = abs(readmatrix('IrrRecorded.csv')');
heatFlowArr = zeros(nDataPoints,1);

delete 'heatFlowInteractionBetween.xls'; delete 'heatFlowNoInteraction.xls';
writematrix([0 0 0 0 0 ; 0 0 0 0 0],'heatFlowInteractionBetween.xls');
writematrix([0 0 0 0 0 0 0; 0 0 0 0 0 0 0],'heatFlowNoInteraction.xls');

% boundary conditions
T_a0 = 15;
T_c0 = 10;
T_f0 = 10;
Y0 = [T_a0 T_c0 T_f0];
t0 = [0 0 0 0]; % initial time

tspan = [1:nDataPoints];
f = @(t, dYdt) ODEEqns(t, dYdt(1), dYdt(2), dYdt(3), T_o, T_s, Irr, rh,
    windSpeed, nDataPoints, floorRad);
[t, dYdt] = ode45(f, tspan, Y0);

% plot various tempertures
plot(T_aRec, LineStyle='--'); hold on;
plot(t, real(dYdt(:,1))); hold off;
grid on; legend('Internal air (meas.)', 'Internal air (pred.)'); xlabel('t, 5m
    intervals'); ylabel('temperature, C'); xlim([0 nDataPoints])

plot(T_o, LineStyle='--'); hold on;
plot(T_s, LineStyle=':'); hold on;
plot(t, real(dYdt(:,2)), LineStyle='-.'); hold on;
plot(t, real(dYdt(:,3))); hold off;
grid on; legend('External air', 'Soil', 'Cover', 'Floor'); xlabel('t, 5m
    intervals'); ylabel('temperature, C'); xlim([0 nDataPoints]);

plot(T_aRec, LineStyle='--'); hold on; plot(T_o, LineStyle='-.'); hold on; plot(
    t, real(dYdt(:,1))); hold off; grid on; legend('meas. int. temp', 'meas. ext
    . temp', 'pred. int. temp'); xlabel('t, 5m intervals'); ylabel('temperature,
     C'); xlim([0 nDataPoints])
```

```
plot(Irr); grid on; legend('meas. irradiance'); xlabel('t, 5m intervals');
    ylabel('Irradiance incident on cover, W'); xlim([0 nDataPoints])
plot(rh); grid on; legend('meas. relative humidity'); xlabel('t, 5m intervals');
     ylabel('Relative humidity, %'); xlim([0 nDataPoints])

% plot individual heat transfer components
plot(readmatrix('heatFlowInteractionBetween.xls')); grid on; legend('Q_{f\_c}',
    'Q_{a\_c}', 'Q_{s\_f}', 'Q_{f\_a}', 'Q_{f\_sh}'); xlabel('t, ODE solution
    step'); ylabel('Heat flow, W');
plot(readmatrix('heatFlowNoInteraction.xls')); grid on; legend('Q_{a\_o}', 'Q_{
    rd\_c}', 'Q_{c\_o}', 'Q_{c\_sk}', 'Q_{rd\_f}', 'Q_{s\_h}', 'Q_{h\_a}');
    xlabel('t, ODE solution step'); ylabel('Heat flow, W');

% calculate error, MAE, and RMSE
error = abs(abs(dYdt(:,1)) - T_aRec); % error vector
MAE = 1/length(error) * sum(error); % mean absolute error
RMSE =  sqrt(1/length(error) * sum(error.^2)); % root mean square error

% plot various errors
plot(error); hold on;
plot(ones(1, nDataPoints) .* MAE); hold on;
plot(ones(1, nDataPoints) .* RMSE); hold off;
grid on; legend('Absolute error', append('MAE=', string(MAE)), append('RMSE=',
    string(RMSE))); xlabel('t, 5m intervals'); ylabel('Error (|meas. - pred.|),
    C'); xlim([0 nDataPoints])

function dYdt = ODEEqns(t, T_a, T_c, T_f, T_o, T_s, rad, rh, windSpeed,
    nDataPoints, floorRad)

% define constants ----------------------------------------
    % global
    rhInterp  = interp1(rh, t);
    T_sInterp = interp1(T_s, t);
    T_oInterp = interp1(T_o, t);
    radInterp = interp1(rad, t);
    floorRadInterp = interp1(floorRad, t);
    windInterp = interp1(windSpeed, t);
    g = 9.806;
    stefBoltzConst = 5.67e-08; % W m-2 K-4
    T_sky = 0.0552*((T_oInterp+273.15)^1.5);
    E_sk = 0.77+0.0038*(T_oInterp - ((1 - rhInterp)/5));

    % internal air
    T_aK      = T_a + 273.15;
    rho_a     = 1.233; % kg/m3, assumed constant, although eqn. 28 can be used
    c_pa      = 1000*( 1.005 + 1.82*((6.112*rhInterp*2.1674*exp(17.67*T_a/(T_a
    +243.5)))/(T_aK)) ); % eqn. 32
    V_a       = 187;  % m3
    N_a       = 60; % guess
    k_a       = (T_aK^(3/2) * 0.00264638)/(T_aK + 245.4*10^(-12/T_aK)); % W/m2
    eta_rda   = 0.05;

    % cover
    rho_c     = 2500; % kg/m3
    c_pc      = 840;  % J/(kg K)
    d_c       = 0.003; % m
    A_c       = 157; % m2
    V_c       = A_c*d_c; % m3
    k_c       = 0.8; % W/(m K)
    alpha_co  = 1.2*windInterp + 2;
    eta_rdc   = 0.02;
    I_c       = radInterp; % W, solar radiation incident on the cover as a
    function of time of day
```

```
    E_c       = 0.93;
    F_csk     = 0.7;

    % floor
    rho_f     = 2500; % kg/m3
    c_pf      = 880;  % J/(kg K)
    k_f       = 1.74;  % W/m2
    d_f       = 0.05; % floor depth, m
    W_f       = 4.4; % width, m
    L_f       = 15.5; % length, m
    A_f       = L_f*W_f; % area, m2
    V_f       = A_f*d_f; % volume, m3
    Pr        = -0.000234*T_a + 0.735; % easier to use linear fit
    mu        = (1.458e-06 * T_aK^(3/2))/(T_aK + 110.4);
    nu        = mu/rho_a;
    delta     = A_f/(2*W_f + 2*L_f);
    Gr        = (g*(1/T_aK)*(T_f-T_a)*delta^3)/nu^2;
    Ra        = Gr*Pr;
    E_f       = 0.85;
    F_fc      = 1;

    if (Ra > 1e04) && (Ra < 1e07)
        Nu    = 0.54*Ra^(1/4);
    else
        Nu    = 0.15*Ra^(1/3);
    end

    h_f       = (Nu*k_a*(2*W_f + 2*L_f))/A_f; % <-- this may be the source of the
     complex numbers...

    % shed
    k_shSideWall = 3; % therm conductivity, W/(m K)
    d_shSideWall = 0.15; % thickness, m
    A_shSideWall = 13*2; % area, m2
    k_shBackWall = 0.08; % can overestimate here as slats allow for ventilation
    not otherwise considered.
    d_shBackWall = 0.015;
    A_shBackWall = 3.8*2.2; % approximate
    k_shRoof   = 0.066;
    d_shRoof   = 0.028;
    A_shRoof   = 1.5*1.92*2; % underestimate as treating as flat
    A_shFloor  = 0.5*24.7; % m2
    A_sh       = A_shRoof + A_shBackWall + 2*A_shSideWall;

% heat flow terms ----------------------------------------
    % internal air
    Q_ao  = (c_pa*N_a*V_a*rho_a*(T_a-T_oInterp))/3600;
    Q_rda = eta_rda*radInterp;

    % cover
    Q_rdc = eta_rdc*I_c*1.5; % assume half of radiation striking cover restrikes
     on the other side
    Q_fc  = A_f*E_f*E_c*F_fc*stefBoltzConst*((T_f+273.15)^4 - (T_c+273.15)^4);
    Q_ac  = A_c*(3*abs(T_a-T_c)^(1/3))*(T_a-T_c);
    Q_co  = A_c*alpha_co*(T_c-T_oInterp);
    Q_csk = A_c*E_c*E_sk*F_csk*stefBoltzConst*((T_c+273.15)^4 - (T_sky)^4);

    % floor
    Q_sf  = k_f*A_f*(T_sInterp-T_f);
    Q_fa  = h_f*A_f*(T_f-T_a);
    Q_fsh = h_f*A_shFloor*(T_f-T_a);
    Q_rdf = floorRadInterp*A_f;
```

```
    % shed
    Q_sh = 2*((k_shSideWall*A_shSideWall*(T_oInterp-T_a))/d_shSideWall) + ...
            + (k_shBackWall*A_shBackWall*(T_oInterp-T_a))/d_shBackWall + ...
            + (k_shRoof*A_shRoof*(T_oInterp-T_a))/d_shRoof ...
            + 0.2*radInterp; % 2 side walls + back wall + roof

    % solar thermal collector
    Q_ha = 0; % no energy added to system

writematrix([Q_fc Q_ac Q_sf Q_fa Q_fsh],'heatFlowInteractionBetween.xls','
    WriteMode','append');
writematrix([Q_ao Q_rdc Q_co Q_csk Q_rdf Q_sh Q_ha],'heatFlowNoInteraction.xls',
    'WriteMode','append');
% equations ------------------------------------------------
dT_adt = (Q_fa -Q_ac +Q_rda +Q_ha -Q_ao +Q_sh)/(rho_a*c_pa*V_a);
dT_cdt = (Q_rdc +Q_fc +Q_ac -Q_co -Q_csk)/(rho_c*c_pc*V_c);
dT_fdt = (Q_sf -Q_fa +Q_rdf -Q_fsh)/(rho_f*c_pf*V_f);

% combine all differential equations into one function
dYdt = [dT_adt; dT_cdt; dT_fdt];
end
```

Code Listing 3: The MATLAB code used to obtain the results presented in this report.

14 References

[1] ICaRE4Farms, "Icare4farms." [Online]. Available: https://www.linkedin.com/company/icare4farms/posts/?feedView=all

[2] ICaRE4Farms and U. of Lincoln, "Icare4farms (i4f) project." [Online]. Available: https://www.lincoln.ac.uk/engineering/research/icare4farms/

[3] Z. Naghibi, R. Carriveau, and D. S.-K. Ting, "Improving clean energy greenhouse heating with solar thermal energy storage and phase change materials," *Energy Storage*, vol. 2, no. 1, p. e116, 2020. [Online]. Available: https://onlinelibrary.wiley.com/doi/10.1002/est2.116

[4] O. Körner, M. Bakker, and E. Heuvelink, "Daily temperature integration: a simulation study to quantify energy consumption," *Biosystems Engineering*, vol. 87, no. 3, pp. 333–343, 2004. [Online]. Available: https://www.sciencedirect.com/science/article/pii/S1537511003002113

[5] M. Souliotis, Y. Tripanagnostopoulos, and A. Kavga, "The use of fresnel lenses to reduce the ventilation needs of greenhouses," in *International Symposium on Greenhouse Cooling 719*, 2006, pp. 107–114. [Online]. Available: https://www.actahort.org/books/719/719_9.htm

[6] G. Vox, E. Schettini, A. Lisi Cervone, and A. Anifantis, "Solar thermal collectors for greenhouse heating," in *International Symposium on High Technology for Greenhouse System Management: Greensys2007 801*, 2007, pp. 787–794. [Online]. Available: https://www.actahort.org/books/801/801_92.htm

[7] M. Esen and T. Yuksel, "Experimental evaluation of using various renewable energy sources for heating a greenhouse," *Energy and Buildings*, vol. 65, pp. 340–351, 2013. [Online]. Available: https://www.sciencedirect.com/science/article/pii/S0378778813003563?via%3Dihub

[8] ICaRE4Farms, "Market outlook of solar thermal energy in north west europe," June 2021. [Online]. Available: https://www.nweurope.eu/media/16131/market-analysis.pdf

[9] A. of the Chambers of Agriculture of the Atlantic Area (AC3A), "Icare4farms - increase the share of renewable energies on farms in north-west europe through the use of solar thermal energy." [Online]. Available: https://ac3a.fr/en/icare4farms-en/

[10] V. Sethi, K. Sumathy, C. Lee, and D. Pal, "Thermal modeling aspects of solar greenhouse microclimate control: A review on heating technologies," *Solar energy*, vol. 96, pp. 56–82, 2013. [Online]. Available: https://www.sciencedirect.com/science/article/pii/S0038092X13002648?via%3Dihub

[11] C. Van Bavel, T. Takakura, and G. Bot, "Global comparison of three greenhouse climate models," in *Symposium Greenhouse Climate and its Control 174*, 1985, pp. 21–34. [Online]. Available: https://www.actahort.org/books/174/174_1.htm

[12] N. Bennis, J. Duplaix, G. Enéa, M. Haloua, and H. Youlal, "Greenhouse climate modelling and robust control," *Computers and electronics in agriculture*, vol. 61, no. 2, pp. 96–107, 2008. [Online]. Available: https://doi.org/10.1016/j.compag.2007.09.014

[13] H. Hamidane, S. El Faiz, M. Guerbaoui, A. Ed-Dahhak, A. Lachhab, and B. Bouchikhi, "Constrained discrete model predictive control of a greenhouse system temperature," *International Journal of Electrical and Computer Engineering*, vol. 11, no. 2, p. 1223, 2021. [Online]. Available: http://ijece.iaescore.com/index.php/IJECE/article/view/22566

[14] G. Singh, P. P. Singh, P. P. S. Lubana, and K. Singh, "Formulation and validation of a mathematical model of the microclimate of a greenhouse," *Renewable Energy*, vol. 31, no. 10, pp. 1541–1560, 2006. [Online]. Available: https://www.sciencedirect.com/science/article/pii/S0960148105002491

[15] E. Cuce, D. Harjunowibowo, and P. M. Cuce, "Renewable and sustainable energy saving strategies for greenhouse systems: A comprehensive review," *Renewable and Sustainable Energy Reviews*, vol. 64, pp. 34–59, 2016. [Online]. Available: https://doi.org/10.1016/j.rser.2016.05.077

[16] R. V. Singh, S. Kumar, M. Hasan, M. E. Khan, and G. Tiwari, "Performance of a solar still integrated with evacuated tube collector in natural mode," *Desalination*, vol. 318, pp. 25–33, 2013. [Online]. Available: https://doi.org/10.1016/j.desal.2013.03.012

[17] H. Benli and A. Durmuş, "Performance analysis of a latent heat storage system with phase change material for new designed solar collectors in greenhouse heating," *Solar energy*, vol. 83, no. 12, pp. 2109–2119, 2009. [Online]. Available: https://doi.org/10.1016/j.solener.2009.07.005

[18] R. Patil and R. Gawande, "A review on solar tunnel greenhouse drying system," *Renewable and sustainable energy reviews*, vol. 56, pp. 196–214, 2016. [Online]. Available: https://doi.org/10.1016/j.rser.2015.11.057

[19] S. A. Kalogirou, "Solar thermal collectors and applications," *Progress in energy and combustion science*, vol. 30, no. 3, pp. 231–295, 2004. [Online]. Available: https://doi.org/10.1016/j.pecs.2004.02.001

[20] I. Attar, N. Naili, N. Khalifa, M. Hazami, M. Lazaar, and A. Farhat, "Experimental study of an air conditioning system to control a greenhouse microclimate," *Energy conversion and management*, vol. 79, pp. 543–553, 2014. [Online]. Available: https://doi.org/10.1016/j.enconman.2013.12.023

[21] N. Sharma and G. Diaz, "Performance model of a novel evacuated-tube solar collector based on minichannels," *Solar Energy*, vol. 85, no. 5, pp. 881–890, 2011. [Online]. Available: https://doi.org/10.1016/j.solener.2011.02.001

[22] V. Tyagi, S. Kaushik, and S. Tyagi, "Advancement in solar photovoltaic/thermal (pv/t) hybrid collector technology," *Renewable and Sustainable Energy Reviews*, vol. 16, no. 3, pp. 1383–1398, 2012. [Online]. Available: https://doi.org/10.1016/j.rser.2011.12.013

[23] S. B. Kedare and N. B. Desai, "Solar thermal process heat," *Encyclopedia of Sustainable Technologies*, pp. 367–376, 2017.

[24] E. Bellos and C. Tzivanidis, "A review of concentrating solar thermal collectors with and without nanofluids," *Journal of Thermal Analysis and Calorimetry*, vol. 135, no. 1, pp. 763–786, 2019. [Online]. Available: https://link.springer.com/article/10.1007/s10973-018-7183-1

[25] M. I. Hussain and G. H. Lee, "Thermal performance evaluation of a conical solar water heater integrated with a thermal storage system," *Energy conversion and management*, vol. 87, pp. 267–273, 2014. [Online]. Available: https://doi.org/10.1016/j.enconman.2014.07.023

[26] H. H. Sait, J. M. Martinez-Val, R. Abbas, and J. Munoz-Anton, "Fresnel-based modular solar fields for performance/cost optimization in solar thermal power plants: A comparison with parabolic trough collectors," *Applied Energy*, vol. 141, pp. 175–189, 2015. [Online]. Available: https://doi.org/10.1016/j.apenergy.2014.11.074

[27] M. Sabiha, R. Saidur, S. Mekhilef, and O. Mahian, "Progress and latest developments of evacuated tube solar collectors," *Renewable and Sustainable Energy Reviews*, vol. 51, pp. 1038–1054, 2015. [Online]. Available: https://doi.org/10.1016/j.rser.2015.07.016

[28] S. A. Klein and W. A. Beckman, "A general design method for closed-loop solar energy systems," *Solar energy*, vol. 22, no. 3, pp. 269–282, 1979. [Online]. Available: https://doi.org/10.1016/0038-092X(79)90142-7

[29] K. R. Anderson, M. Shafahi, A. Artounian, and A. Chrisman, "Analysis of solar heating system for an aquaponics food production system," *International Journal of Sustainable and Green Energy*, vol. 4, pp. 1–6, 2015. [Online]. Available: http://www.sciencepublishinggroup.com/j/ijrse

[30] L. Malquori, P. Pellegrini, and R. Tesi, "Determination of solar energy transmitted by different greenhouse geometries [tuscany]." *Colture Protette*, 1993. [Online]. Available: https://agris.fao.org/agris-search/search.do?recordID=IT19940059641

[31] A. Rigby, "The burnley low energy greenhouse," *Energy Conservation and Solar Energy Utilization in Horticultural Engineering 257*, pp. 41–54, 1986. [Online]. Available: https://doi.org/10.17660/ActaHortic.1989.257.6

[32] J. S. Haberl and S. Cho, "Literature review of uncertainty of analysis methods (f-chart program), report to the texas commission on environmental quality," 2004. [Online]. Available: https://oaktrust.library.tamu.edu/handle/1969.1/2062

[33] S. A. Kalogirou, *Solar Energy Engineering: Processes and Systems*, 2nd ed. Academic Press, 2013. [Online]. Available: https://www.elsevier.com/books/solar-energy-engineering/kalogirou/978-0-12-397270-5

[34] J. A. Duffie, W. A. Beckman, and J. McGowan, "Solar engineering of thermal processes," *American Journal of Physics*, vol. 53, p. 382, 1985. [Online]. Available: https://aapt.scitation.org/doi/pdf/10.1119/1.14178

[35] J. Boland, L. Scott, and M. Luther, "Modelling the diffuse fraction of global solar radiation on a horizontal surface," *Environmetrics*, vol. 12, pp. 103 – 116, 03 2001. [Online]. Available: https://www.researchgate.net/publication/229873508_Modelling_the_diffuse_fraction_of_global_solar_radiation_on_a_horizontal_surface

[36] T. Muneer, S. Etxebarria, and E. Gago, "Monthly averaged-hourly solar diffuse radiation model for the uk," *Building Services Engineering Research and Technology*, vol. 35, no. 6, pp. 573–584, 2014. [Online]. Available: https://www.napier.ac.uk/~/media/worktribe/output-175455/monthly-averaged-hourly-solar-diffuse-radiation-model-for-the-uk.pdf

[37] M. Hofmann and G. Seckmeyer, "A new model for estimating the diffuse fraction of solar irradiance for photovoltaic system simulations," *Energies*, vol. 10, no. 2, p. 248, 2017. [Online]. Available: https://www.mdpi.com/1996-1073/10/2/248

[38] G. Bourges, "Reconstitution des courbes de fréquence cumulées de l'irradiation solaire globale horaire reçue par une surface plane," *Report CEE*, vol. 295, p. 77, 1979.

[39] J. Duffie and W. Beckman, *Solar Energy Thermal Processes*, 4th ed., ser. A Wiley-Interscience publication. Wiley, 2013. [Online]. Available: https://www.wiley.com/en-gb/Solar+Engineering+of+Thermal+Processes%2C+4th+Edition-p-9780470873663

[40] J. Boland, B. Ridley, and B. Brown, "Models of diffuse solar radiation," *Renewable Energy*, vol. 33, no. 4, pp. 575–584, 2008. [Online]. Available: https://www.sciencedirect.com/science/article/pii/S0960148107001267

[41] A. Sánchez de Miguel, M. Aubé, J. Zamorano, M. Kocifaj, J. Roby, and C. Tapia, "Sky Quality Meter measurements in a colour-changing world," *Monthly Notices of the Royal Astronomical Society*, vol. 467, no. 3, pp. 2966–2979, 03 2017. [Online]. Available: https://doi.org/10.1093/mnras/stx145

[42] G. Zhang, X. Ding, T. Li, W. Pu, W. Lou, and J. Hou, "Dynamic energy balance model of a glass greenhouse: An experimental validation and solar energy analysis," *Energy*, vol. 198, p. 117281, 2020. [Online]. Available: https://www.sciencedirect.com/science/article/pii/S0360544220303881

[43] R. J. van Ooteghem, "Optimal control design for a solar greenhouse," *IFAC Proceedings Volumes*, vol. 43, no. 26, pp. 304–309, 2010, 3rd IFAC Conference in Modelling and Control in Agriculture, Horticulture and Post-Harvest Processing - Agricontrol. [Online]. Available: https://www.sciencedirect.com/science/article/pii/S147466701531082X

[44] G. Van Straten, G. van Willigenburg, E. van Henten, and R. van Ooteghem, *Optimal control of greenhouse cultivation*. CRC Press, 2010. [Online]. Available: https://doi.org/10.1201/b10321

[45] R. Shelquist, "An introduction to air density and density altitude calculations," 2019. [Online]. Available: https://wahiduddin.net/calc/density_altitude.htm

[46] Çengel, Boles, and Kanoğlu, *Thermodynamics, an Engineering Approach*, 9th ed. McGraw-Hill Education, 2019.

[47] V. Group, "Humidity conversion formulas: Calculation formulas for humidity," 2013. [Online]. Available: https://www.hatchability.com/Vaisala.pdf

[48] P. Mander, "Formula for calculating absolute humidity," 2012. [Online]. Available: https://carnotcycle.wordpress.com/2012/08/04/how-to-convert-relative-humidity-to-absolute-humidity/

[49] I. Al-Helal, S. Waheeb, A. Ibrahim, M. Shady, and A. Abdel-Ghany, "Modified thermal model to predict the natural ventilation of greenhouses," *Energy and Buildings*, vol. 99, pp. 1–8, 2015. [Online]. Available: https://www.sciencedirect.com/science/article/pii/S0378778815003126

[50] J. Du, P. Bansal, and B. Huang, "Simulation model of a greenhouse with a heat-pipe heating system," *Applied Energy*, vol. 93, pp. 268–276, 2012, (1) Green Energy; (2)Special Section from papers presented at the 2nd International Enery 2030 Conf. [Online]. Available: https://www.sciencedirect.com/science/article/pii/S0306261911008725

[51] M. Taki, Y. Ajabshirchi, S. F. Ranjbar, A. Rohani, and M. Matloobi, "Modeling and experimental validation of heat transfer and energy consumption in an innovative greenhouse structure," *Information Processing in Agriculture*, vol. 3, no. 3, pp. 157–174, 2016. [Online]. Available: https://www.sciencedirect.com/science/article/pii/S2214317316300105

[52] M. Mirsadeghi, D. Cóstola, B. Blocken, and J. Hensen, "Review of external convective heat transfer coefficient models in building energy simulation programs: Implementation and uncertainty," *Applied Thermal Engineering*, vol. 56, no. 1, pp. 134–151, 2013. [Online]. Available: https://www.sciencedirect.com/science/article/pii/S1359431113001543

[53] W. C. Swinbank, "Long-wave radiation from clear skies," *Quarterly Journal of the Royal Meteorological Society*, vol. 89, no. 381, pp. 339–348, 1963. [Online]. Available: https://rmets.onlinelibrary.wiley.com/doi/epdf/10.1002/qj.49708938105

[54] ANSYS, Inc., "View factors - thermal radiation in heat transfer analysis – lesson 2." [Online]. Available: https://courses.ansys.com/wp-content/uploads/2020/05/Lesson-2-View-factors.pdf

[55] M. R. Vujičić, N. P. Lavery, and S. G. R. Brown, "View factor calculation using the monte carlo method and numerical sensitivity," *Communications in Numerical Methods in Engineering*, vol. 22, no. 3, pp. 197–203, 2006. [Online]. Available: https://onlinelibrary.wiley.com/doi/abs/10.1002/cnm.805

[56] C. McKinstry, "View factors: What they are and how to calculate them," August 2021. [Online]. Available: https://summerofhpc.prace-ri.eu/view-factors-what-they-are-and-how-to-calculate-them/#:~:text=In%20this%20case%2C%20one%20can,%3E%20FdA1%20%2D%3E%20A2.

[57] O. Gliah, B. Kruczek, S. G. Etemad, and J. Thibault, "The effective sky temperature: An enigmatic concept," *Heat and Mass Transfer*, vol. 47, pp. 1171–1180, 09 2011.

[58] X. Berger, D. Buriot, and F. Garnier, "About the equivalent radiative temperature for clear skies," *Solar Energy*, vol. 32, no. 6, pp. 725–733, 1984.

[59] M. G. Lawrence, "The relationship between relative humidity and the dewpoint temperature in moist air: A simple conversion and applications," *Bulletin of the American Meteorological Society*, vol. 86, no. 2, pp. 225–234, 2005.

[60] P. Kosky, P. Kosky, W. Keat, and G. Wise, *Exploring Engineering*. Academic Press, 2013. [Online]. Available: https://doi.org/10.1016/C2011-0-04445-9

[61] Engineers Edge, LLC, "Horizontal plate natural convection equations and calculator." [Online]. Available: https://www.engineersedge.com/heat_transfer/horizontal_plate_natural_convection_13968.htm

[62] N. Oceanic, A. Administration, NASA, and U. S. A. Force, "U.s. standard atmosphere, 1976." [Online]. Available: https://www.ngdc.noaa.gov/stp/space-weather/online-publications/miscellaneous/us-standard-atmosphere-1976/us-standard-atmosphere_st76-1562_noaa.pdf

[63] A. Y. Cengel and J. M. Cimbala, *Fluid Mechanics: Fundamentals and Applications*, 1st ed. McGraw-Hill Science/Engineering/Math, 2004. [Online]. Available: https://www.mheducation.com/highered/product/fluid-mechanics-fundamentals-applications-cengel-cimbala/M9781259696534.html

[64] M. Zeneli, A. Nikolopoulos, S. Karellas, and N. Nikolopoulos, "Chapter 7 - numerical methods for solid-liquid phase-change problems," in *Ultra-High Temperature Thermal Energy Storage, Transfer and Conversion*, ser. Woodhead Publishing Series in Energy, A. Datas, Ed. Woodhead Publishing, 2021, pp. 165–199. [Online]. Available: https://www.sciencedirect.com/science/article/pii/B9780128199558000077

[65] W. Zhang, H. Min, X. Gu, Y. Xi, and Y. Xing, "Mesoscale model for thermal conductivity of concrete," *Construction and Building Materials*, vol. 98, pp. 8–16, 2015. [Online]. Available: https://www.sciencedirect.com/science/article/pii/S0950061815303238

[66] K.-H. Kim, S.-E. Jeon, J.-K. Kim, and S. Yang, "An experimental study on thermal conductivity of concrete," *Cement and Concrete Research*, vol. 33, no. 3, pp. 363–371, 2003. [Online]. Available: https://www.sciencedirect.com/science/article/pii/S0008884602009651

[67] I. Asadi, P. Shafigh, Z. F. B. Abu Hassan, and N. B. Mahyuddin, "Thermal conductivity of concrete – a review," *Journal of Building Engineering*, vol. 20, pp. 81–93, 2018. [Online]. Available: https://www.sciencedirect.com/science/article/pii/S2352710218304650

[68] E. ToolBox, "Absorbed solar radiation," 2009. [Online]. Available: https://www.engineeringtoolbox.com/solar-radiation-absorbed-materials-d_1568.html

[69] M. Grahovac, P. Liedl, J. Frisch, and P. Tzscheutschler, "Simplified solar collector model: Hourly simulation of solar boundary condition for multi-energy optimization," 12 2010.

[70] P. Kovacs and SP, "A guide to the standard en 12975," 2012. [Online]. Available: http://www.estif.org/fileadmin/estif/content/projects/QAiST/QAiST_results/QAiST%20D2.3%20Guide%20to%20EN%2012975.pdf

[71] D. Burnett, E. Barbour, and G. P. Harrison, "The uk solar energy resource and the impact of climate change," *Renewable Energy*, vol. 71, pp. 333–343, 2014. [Online]. Available: https://www.sciencedirect.com/science/article/pii/S0960148114002857

[72] J. Botero-Valencia, M. Mejia-Herrera, and J. M. Pearce, "Design and implementation of 3-d printed radiation shields for environmental sensors," *HardwareX*, vol. 11, p. e00267, 2022. [Online]. Available: https://www.sciencedirect.com/science/article/pii/S2468067222000128

[73] T. Chai and R. R. Draxler, "Root mean square error (rmse) or mean absolute error (mae)?–arguments against avoiding rmse in the literature," *Geoscientific model development*, vol. 7, no. 3, pp. 1247–1250, 2014.

[74] C. J. Willmott and K. Matsuura, "Advantages of the mean absolute error (mae) over the root mean square error (rmse) in assessing average model performance," *Climate research*, vol. 30, no. 1, pp. 79–82, 2005.

[75] C. Kittas, T. Boulard, and G. Papadakis, "Natural ventilation of a greenhouse with ridge and side openings: sensitivity to temperature and wind effects," *Transactions of the ASAE*, vol. 40, no. 2, pp. 415–425, 1997.

[76] M. C. Singh, J. Singh, and K. Singh, "Development of a microclimate model for prediction of temperatures inside a naturally ventilated greenhouse under cucumber crop in soilless media," *Computers and Electronics in Agriculture*, vol. 154, pp. 227–238, 2018. [Online]. Available: https://www.sciencedirect.com/science/article/pii/S016816991830022X

[77] H. England, "Parish church of st mary." [Online]. Available: https://historicengland.org.uk/listing/the-list/list-entry/1064120